R2 Resource Consultants, Inc.

15250 NE 95th Street
Redmond, WA 98052-2518
Phone: (425) 556-1288
Fax: (425) 556-1290
e-mail: mail@R2usa.com

Technical Memorandum

Date: July 6, 2010 Project Number: 1771.01/MM101

To: Bob Aldrich, Snohomish County Surface Water Management

From: Paul DeVries, Ph.D., P.E., Chiming Huang, Ph.D., P.E.

Subject: Reach Scale Geomorphic Analysis of Hydraulic, Hydrologic, and Sediment Conditions in the Lower South Fork Stillaguamish River Below Canyon Creek

CONTENTS

1. INTRODUCTION

R2 Resource Consultants Inc, (R2) is assisting Snohomish County Surface Water Management (SWM) with reach scale geomorphic analyses that will be used to support assessment and prioritization of river and fish habitat restoration possibilities in the lower South Fork Stillaguamish River reach, extending between confluences with Canyon Creek at the upstream end near Granite Falls, and with the North Fork Stillaguamish River at the downstream end near Arlington (Figure 1). The analyses are intended to facilitate identifying restoration projects that address restoration needs identified in the 2005 Stillaguamish Watershed Chinook Salmon Recovery Plan, are consistent and compatible with natural reach scale hydraulic and sediment transport processes and will restore and protect salmon habitat as well as protect infrastructure in the reach**.** R2 worked closely with SWM staff in the collection and analysis of data specific to the reach geomorphic assessment and directed at the following goals:

1. Identify reach scale processes that influence channel morphology;
2. Identify hydraulic and sediment transport processes that will influence future condition and channel location in the reach;
3. Identify the most geomorphically active and inactive segments in the reach; and
4. Qualify risk associated with different restoration activities for each level of geomorphic activity, including channel connectivity, floodplain connectivity, instream/bank stabilization structures, and bank revetment removal.

The conceptual framework for the analysis is that specific project types will have highest probability of success if they are matched to the dominant reach scale geomorphic processes that affect their function. For example, projects that provide habitat more commonly found under dynamic channel shifting conditions have highest probability of functioning properly when they are located where hydraulic and sediment transport processes strongly favor deposition of sediments. These segments tend to be most active geomorphically. Conversely, projects that provide instream habitat structure will function best when they are located in reaches that are in approximate equilibrium in terms of sediment transport and channel movement (i.e., most inactive geomorphically).

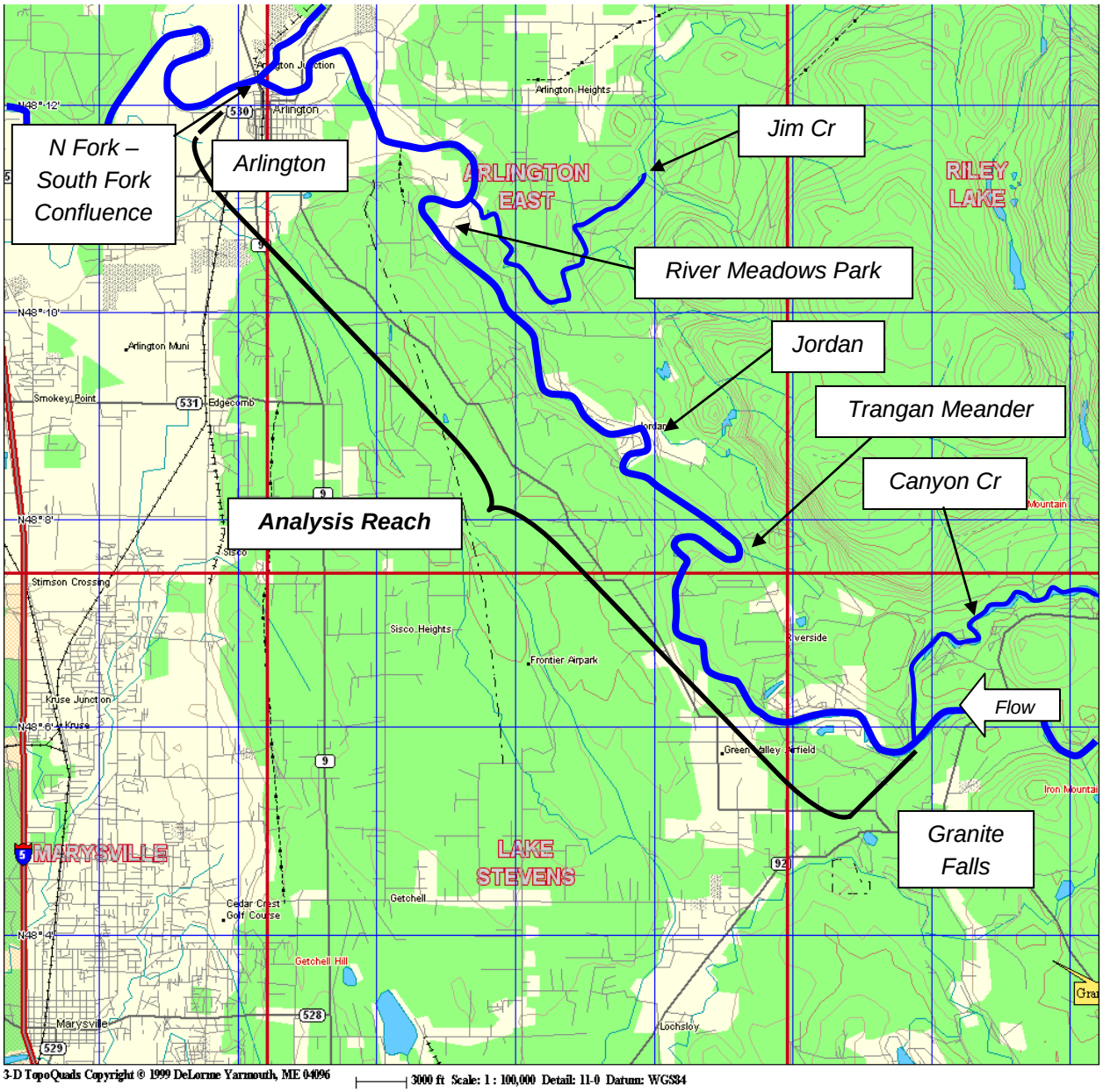

Figure 1. Location of the lower South Fork Stillaguamish River reach analyzed in this memorandum, between Granite Falls and Arlington, WA.

The geomorphic analysis was developed to characterize such reach scale processes and risk, and involved the following elements that are described in this memorandum:

1. Collection and analysis of pebble count data, and analysis of long profile characteristics.
2. Development of a HEC-RAS model for use in hydraulic and sediment transport analyses relative to identifying river segments with aggradational vs. degradation tendencies and for estimating hydraulic characteristics at various flow levels.
3. Digitizing of former main and side channel locations and unvegetated gravel bars using available aerial photography up to and including 2007, and calculating channel migration rates and changes in active gravel bar areas
4. Delineation of potential floodplain avulsion channels and assessment of avulsion risks.
5. Review and synthesis of the sediment transport, channel migration rate, and gravel bar data to develop ratings for each parameter for sub-reaches within the project reach (called analysis segments).
6. Identification of appropriate restoration project types for different segments based on segment characteristics developed in the preceding tasks.

The work products will be used to guide future specific restoration grant applications for completing projects that are consistent with natural geomorphic processes in the lower South Fork Stillaguamish River. This work is generally consistent with work conducted in the Sauk and Skykomish rivers.

The analysis reach is roughly 16½ miles long and provides particularly important spawning and rearing habitat for South Fork Stillaguamish River fall Chinook salmon (*Oncorhynchus tshawytscha*), one of two distinct Chinook stocks identified as being important for recovery in the basin and for which escapement numbers are estimated at 7% of historic levels based on habitat capacity assessments as reported in the 2005 Stillaguamish Watershed Chinook Salmon Recovery Plan.

Key components identified by the Recovery Plan are to restore and preserve watershed processes, improve preferred spawning area, and provide juvenile rearing habitat along mainstem river margins in confined sections of the mainstem and off-channel floodplain habitats in unconfined sections. The analyses documented in this memo are key to understanding the reach scale processes that control the distribution, quality, and persistence of mainstem spawning and

juvenile habitat. Projects that increase mainstem and side channel habitat availability and quality are considered desirable for enabling recovery of Chinook salmon stocks in the basin.

The work and results described in this memorandum can be used to assess opportunities and risks of specific restoration activities designed to improve juvenile and spawning habitats, as well as more general risks to floodplain development and infrastructure. To accomplish this, a strategy was employed of identifying the extent to which shorter, distinct segments within the reach are geomorphically active (or inactive) in terms of sediment transport, deposition, channel migration, and overall erosion tendency. This strategy allowed evaluation of specific locations on the floodplain in the context of local and reach scale constraints. In addition, the results facilitate explanation of the physical cause of specific effects to infrastructure and private land in an intuitive way to stakeholders.

2. METHODS

A suite of analyses was selected over focusing on a specific method, any one of which on its own would provide some information but would not yield a sufficiently complete picture. Quantitative, process-based analyses (e.g., sediment transport modeling, bank migration rates, gravel bar areas) were favored over channel form (e.g., see Kondolf et al. 2001) or process-based classifications (e.g., channel migration zone mapping; Rapp and Abbe 2003), so that the results could be used to better answer the question, "What would happen if…" The analysis involved identifying and quantifying (1) physical processes that influence reach channel morphology, (2) hydraulic and sediment transport processes that will affect future condition and channel location in the reach, and (3) the most geomorphically active and inactive segments in reach. To accomplish these tasks, information was analyzed that was critical for assessing processes acting at the reach and site scales (Wissmar and Beschta 1998; Kondolf 2000): (1) longitudinal profiles of elevation, gradient, and grain size distributions, (2) hydraulics and hydrology using HEC-RAS, USGS gage data, and surveyed cross-section and flood stage data, (3) bedload transport potential based on a 50-year duration, (4) aerial photographs for changes in active channel locations and cumulative active gravel bar storage and side channel areas, and (5) LiDAR and other available GIS data for characterizing flood engagement frequency and avulsion risk potential of floodplain channels. Important details of the methods are described below.

2.1 Longitudinal Profiles

Longitudinal profiles provide an indication of effects of large scale slope changes on sediment transport and deposition patterns. Longitudinal profiles were developed for water surface and thalweg elevations and mean velocity over the analysis reach and upstream, using the HEC-RAS model data and predictions for the 2-yr flood event. The HEC-RAS model water surface elevation data were also used to generate stream gradient profiles. The longitudinal profiles were used to identify general sediment transport trends in the reach.

A total of 21 pebble counts were sampled to characterize upstream-downstream variation in grain size and depositional patterns in the reach, and compare with upstream data collected previously. It was generally not feasible to collect data near the thalweg given channel size. Instead, a sample size of 100 stones was selected randomly by moving over the mid-point of active depositional point bars between the water and floodplain and measuring the intermediate axis diameter of each stone. Sampling locations were selected to be geomorphically similar in terms of bar type and relative location on the bar, so that observed longitudinal variation in grain sizes would not reflect locally variable depositional processes, but rather larger scale geomorphic

variation. Various percentile particle sizes, including D_{50} (size for which 50 percent of stones were smaller), were computed for each sample and plotted against river mile. Inspection of the longitudinal scatter in D_{50} and D_{90} values indicated that there were three sub-reaches in the plot corresponding to large scale breaks in channel confinement and flood flows. Pebble count data were accordingly pooled within each sub-reach to develop grain size distributions. The resulting three grain size distributions were applied to subsections of the reach modeled in the sediment transport analyses.

2.2 Sediment Transport Modeling

Sediment transport modeling involved first creating a hydraulic HEC-RAS model of the reach and using the model output to predict sediment transport rates within the active channel, and develop a within-reach sediment transport budget.

2.2.1 HEC-RAS Model Geometric Data

A HEC-RAS steady flow model was constructed to simulate bedload transporting flood flows and predict longitudinal shear stress variation for estimating bedload transport rates and their effect on a coarse sediment budget within the analysis reach. The model was developed using bathymetric longitudinal and cross-section profile data collected in the field by County staff and LiDAR data. All elevations were calculated relative to the NAVD 88 vertical datum. Benchmarks were established and tied-in using real time kinematic (RTK) GPS and a total station. Profile data were collected using a raft that was rowed across channel. Cables were not used to maintain position, and thus the data did not represent a perfectly straight line, which is needed for computing flow rate and stage in HEC-RAS. To account for this, the surveyed profile bed elevations were projected onto straight transect lines in GIS. Elevations were computed by subtracting the water depth from the water surface elevation, which was determined using RTK GPS. The bare earth model LiDAR data were used to complete dry-land portions including exposed bars, side channels, and the floodplain.

The upstream and downstream boundary conditions were approximated in HEC-RAS using the normal depth assumption in lieu of having measured rating curves. A real-time stream gage has been monitored by Washington Department of Ecology (DOE) since 2004. The gage is located near the upstream boundary and was thus used to help calibrate the model and evaluate water surface elevation predictions. Transect spacing was specified in the HEC-RAS model for the channel centerline, and shoreward of the left and right banks. Transect names were set equal to centerline stationing using a river mile designation. Left and right bank longitudinal stationings were measured on scaled color aerial photographs using GIS. Ineffective flow areas were

specified at selected transects to help distribute the flow better or to delay engagement of side channels and floodplain areas until higher flows, based on review of aerial photographs and assessing land cover and side-channel size characteristics. The model cross-sections (Figure 2) generally defined "analysis segments" for which other quantities were calculated such as bank migration rate and gravel bar area. There were also a few transects added later in the analysis to improve model accuracy that did not define analysis segments. Table 1 lists the analysis river mile for each HEC-RAS model transect defining an analysis segment, and Plate 1 depicts the corresponding analysis segment locations.

2.2.2 HEC-RAS Model Calibration

The HEC-RAS model was calibrated using water surface elevations surveyed for three flows, 17,800 cfs, 8,330 cfs, and 500 cfs at the DOE gage (Station No. 05A105). The first two flows corresponded to peak events that occurred during the 2009-2010 winter and for which high water marks could be discerned in the field. Discharge accretion was neglected in the reach. The flow contribution of Jim Creek to mainstem flow downstream is approximately 7% at the 10 and 50 year flood levels according to the FEMA Flood Insurance Study completed in 2005. Errors involved in modeling of bedload transport imbalances between transects and of avulsion flow risks should therefore be generally minor and not affect the overall results of the study meaningfully in the context of predicting longitudinal variation in sediment transport potential. The model should not be considered accurate for predicting water levels that can be used to delineate the 100-year floodplain per FEMA standards, although the predicted levels should be approximately correct for assessing avulsion risk ratings (see below).

High water surface elevations were marked and surveyed with RTK GPS by R2 and SWM staff in the field at various locations along the river. Peak flood stage marks were indicated as wash and debris lines on exposed soils and sand, debris lines in vegetation, vegetation filaments on trees, logs and moss, differential discoloration of tree trunks, erosion of moss on trees, and other indicators. Multiple signs were identified at each cross-section location, and agreed on by three persons as being suitable estimates of the peak stage. Calibration focused primarily on the 17,800 cfs event which occurred on November 17, 2009. That event corresponded to a flood with between 2-5 year recurrence intervals and was thus considered reasonably representative of hydraulic conditions and coarse bedload transport in the main channel during extreme events. Water surface elevation was also surveyed for the flow occurring on the day that high water marks were surveyed to evaluate low flow hydraulics, at around 500 cfs at the DOE gage.

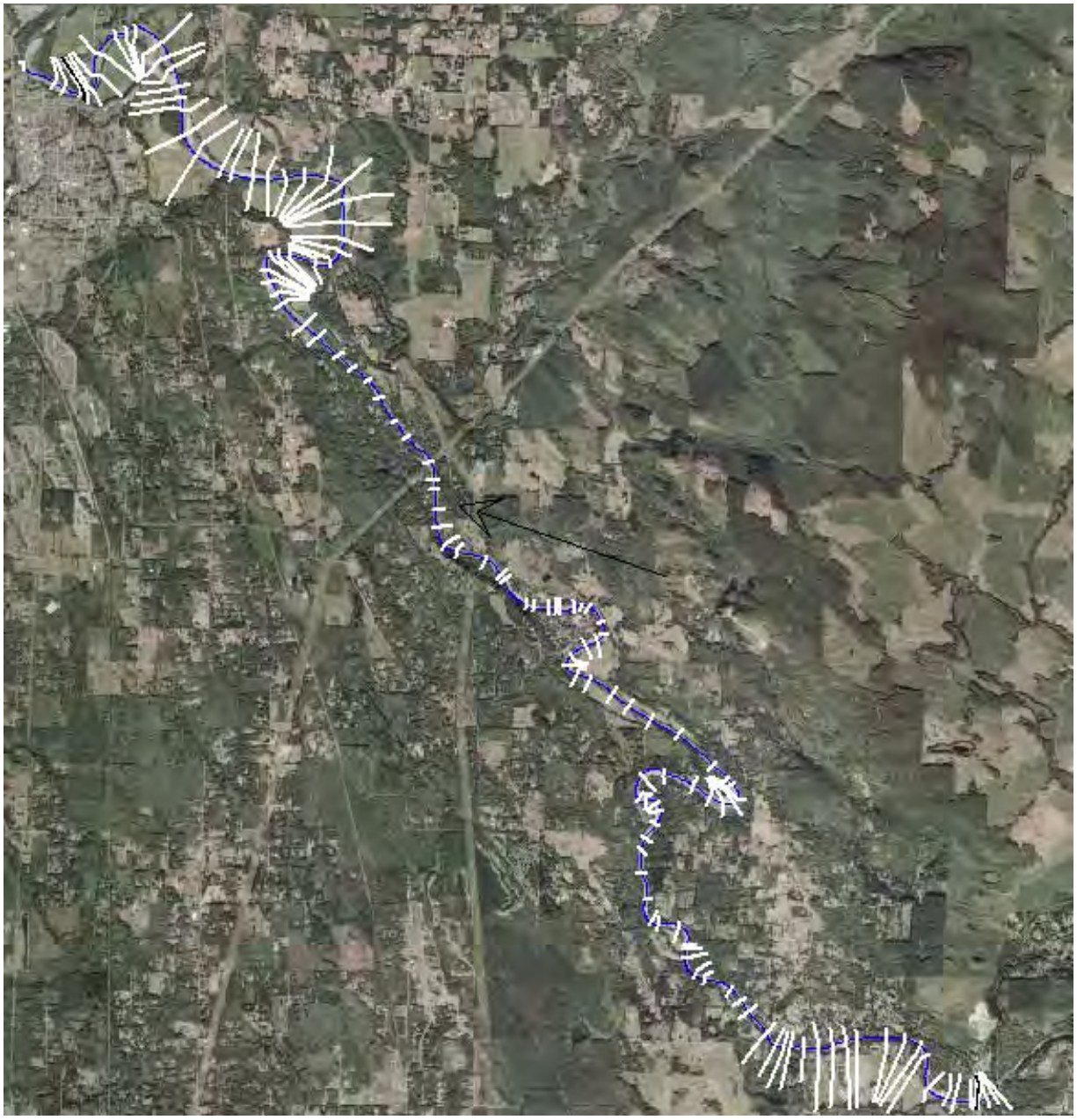

Figure 2. Location of HEC-RAS transects established to predict flood levels and sediment transport rates.

Table 1. River mile (RM) system used in the geomorphic analysis (RM 0 = confluence with North Fork and main Stillaguamish rivers). Analysis segments were used to characterize spatial variation in sediment transport and deposition, and channel migration trends.

Analysis Segment	Analysis RM (Downstream Boundary)	Landmarks, Notes
1	16.40	Jordan Rd Bridge
2	16.34	DOE Stream Gage
3	16.31	
4	16.28	
5	16.09	Island
6	15.93	Island
7	15.82	
8	15.69	
9	15.60	
10	15.34	
11	15.04	
12	14.82	Engebretsen Rd, Top End
13	14.56	
14	14.49	
15	14.37	
16	14.17	
17	14.06	
18	13.95	
19	13.74	
20	13.66	Engebretsen Rd, Bottom End
21	13.41	LDS Camp
22	13.24	
23	13.09	
24	13.04	
25	12.48	
26	12.38	
27	12.26	
28	12.14	
29	12.00	

Table 1. River mile (RM) system used in the geomorphic analysis (RM 0 = confluence with North Fork and main Stillaguamish rivers). Analysis segments were used to characterize spatial variation in sediment transport and deposition, and channel migration trends.

Analysis Segment	Analysis RM (Downstream Boundary)	Landmarks, Notes
30	11.94	
31	11.76	
32	11.58	
33	11.34	
34	11.18	Trangen Meander, Top End
35	11.05	
36	10.91	Trangen Meander, Bottom End
37	10.70	
38	10.36	
39	10.16	
40	9.93	
41	9.58	
42	9.27	
43	9.16	
44	9.08	
45	8.94	
46	8.86	
47	8.78	
48	8.68	
49	8.54	Jordan Footbridge
50	8.48	
51	8.42	Island
52	8.30	Island
53	8.23	
54	8.11	
55	8.04	
56	7.75	
57	7.58	
58	7.36	

Table 1. River mile (RM) system used in the geomorphic analysis (RM 0 = confluence with North Fork and main Stillaguamish rivers). Analysis segments were used to characterize spatial variation in sediment transport and deposition, and channel migration trends.

Analysis Segment	Analysis RM (Downstream Boundary)	Landmarks, Notes
59	7.25	
60	7.11	
61	6.75	Power Lines
62	6.59	
63	6.36	
64	6.31	
65	6.00	
66	5.83	
67	5.49	
68	5.19	River Meadows Park, Top End
69	4.94	
70	4.90	
71	4.83	
72	4.70	
73	4.60	
74	4.50	
75	4.39	
76	4.22	River Meadows Park, Bottom End
77	4.15	Jim Creek
78	3.99	
79	3.90	
80	3.76	
81	3.60	
82	3.49	
83	3.24	
84	2.93	
85	2.80	Power Lines
86	2.55	
87	2.35	

Table 1. River mile (RM) system used in the geomorphic analysis (RM 0 = confluence with North Fork and main Stillaguamish rivers). Analysis segments were used to characterize spatial variation in sediment transport and deposition, and channel migration trends.

Analysis Segment	Analysis RM (Downstream Boundary)	Landmarks, Notes
88	2.17	
89	1.97	
90	1.89	
91	1.81	
92	1.65	Island
93	1.56	Island
94	1.44	
95	1.30	
96	1.22	
97	1.10	
98	1.05	
99	0.86	
100	0.69	
101	0.57	
102	0.50	SR 530 Bridge

Calibration focused first on establishing the order of magnitude of Manning's n-values occurring at the November 2009 peak flow level. Predicted water surface elevations were compared with surveyed values where available to estimate the approximate magnitude of n for high flow in the main channel. The model was then recalibrated to the 8,330 cfs flow level and the 500 cfs level to indirectly confirm the calibration where Manning's n should increase with discharge. The values derived in the peak flow calibration were generally consistent with published values for other rivers with similar channel size and roughness features, and with an estimate of n=0.034-0.038 derived informally using the composite method of Chow (1959). The calibration results were thus considered suitable for modeling of sediment transport flows.

The model was calibrated and run using the interpolated transect feature of HEC-RAS. The extra transects were needed to ensure (i) more reasonable calibration n-values, (ii) reduce modeled head loss between transects to avoid model warning messages re. a 1 ft criterion, and

(iii) increase numerical accuracy. Adding extra transects stabilized the model better by smoothing between-transect changes in depth and velocity, and distributing energy losses across shorter model segments. Interpolated transects were generally spaced less than approximately 200 ft apart, resulting in energy losses between transects generally equal to about 1.0 ft or less at flood stage, a resolution considered sufficient for the river size.

Calibration errors were generally within +/- 0.26 ft at the 17,800 flow level. Results of the HEC-RAS model calibration are provided in Appendix A.

2.2.3 Sediment Transport Simulation Flows

As indicated above, the DOE is monitoring a stream flow gage at the upstream end of the reach below Canyon Creek (Station No. 05A105) but the record (2004-present) is too short to estimate peak flow magnitudes for longer recurrence intervals. The USGS is also monitoring a gage above Canyon Creek since 1928 (Station No. 12161000), but have only reported stage since 1999. The historic flow record for that gage covers the period of 1928-80. The most recent rating curves available for the USGS gage are unlikely to be accurate for much of the low to mid-flow range because of changes in bed topography since 1980. However, gage notes on file suggest relatively little change has likely occurred for higher flows because of bedrock and boulder control downstream at Granite Falls. Thus older rating curves should provide a reasonable working estimate of flood flows today for assessing and adjusting data at the DOE gage for purposes of estimating peak flow magnitudes associated with longer recurrence interval events.

Daily average flows were predicted at the USGS gage from daily average stage using data extracted from a photocopy of an historic rating curve obtained previously by the first author as part of a research project (No. 9; Figure 3), and were then correlated with flows at the DOE gage. This generated a conversion relation for flows at the two mainstem gages (Figure 4). The relation appeared to fit well through the scatter of data and was used to generate a flow duration curve for the reach below Canyon Creek based on the longer period USGS flow data from upstream. The flow duration curve was discretized into a histogram approximating the duration of various simulation flow magnitudes as a percent of the length of the record (Figure 5). The distribution of flows was determined based on matching total volume under the curve and total number of days over a 50-year period while also approximating the curve shape. Flows for the 10-, 25-, and 50 year floods were taken directly from the County's 2005 FIS estimates.

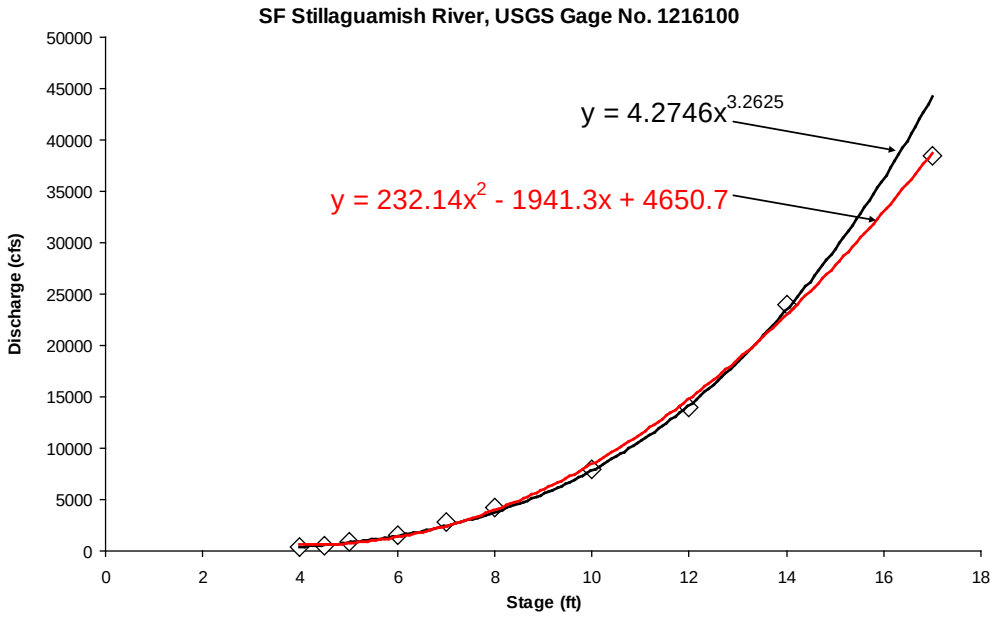

Figure 3. Alternative regressions of stage-discharge rating curve data for USGS gage No. 12161000; the power relation was used to predict flows for stage less than 14.0 ft, and the polynomial for stage greater than 14 ft.

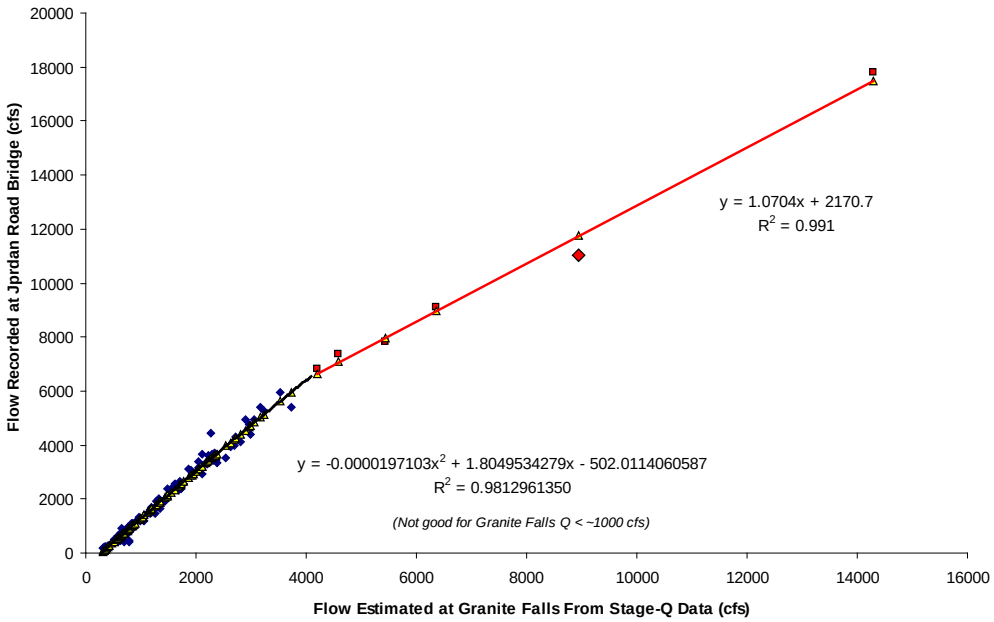

Figure 4. Comparison of average daily flow data and resulting regression curve for the USGS and DOE stream gages on the South Fork Stillaguamish River near Granite Falls.

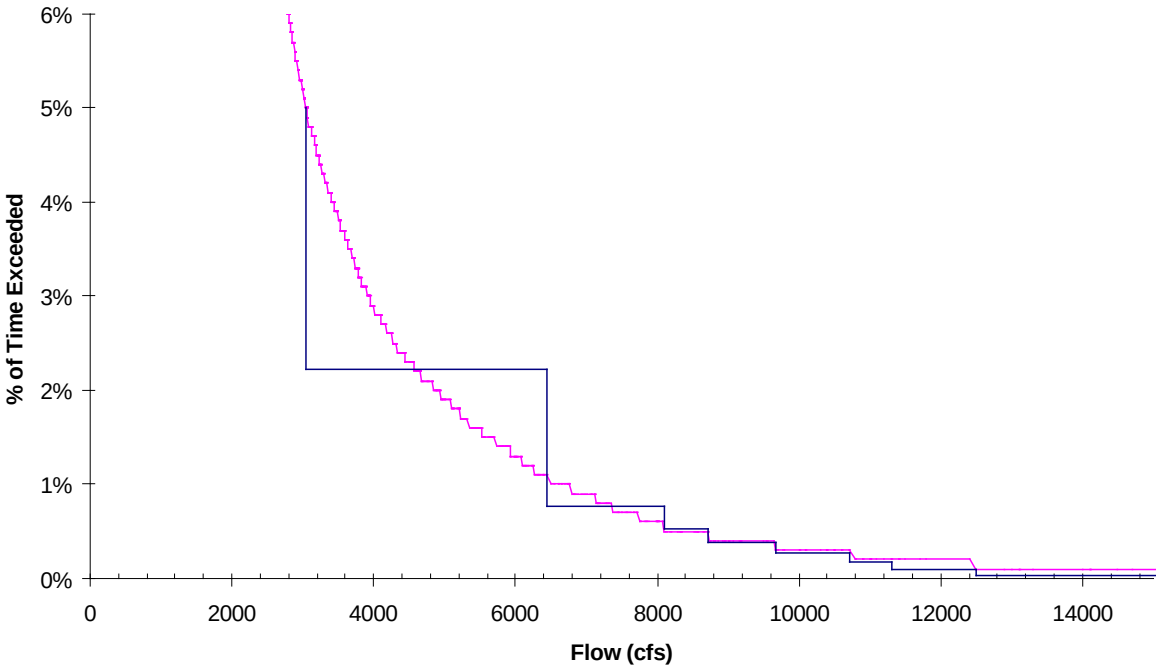

Figure 5. Flow duration curve developed for the analysis reach, and corresponding discretization employed to approximate flow duration for the 50-year bedload transport sediment budget analysis.

2.2.4 Bedload Transport Analysis

The simulation flows were modeled in HEC-RAS using the steady flow option, for a series of discharges equal to and greater than the 5 percent exceedance flow, up to the 50 year flood. Relatively little bedload transport occurs in general in alluvial rivers when discharge is below the 5 percent exceedance flow. A 50-year period was simulated to predict the total volume of bedload transported at each HEC-RAS transect and evaluate corresponding long term deposition and erosion trends in the reach over a representative project design life.

The HEC-RAS main channel shear stress predictions were input with grain size distribution data to a Fortran program that predicted sediment transport rate per unit width based on Parker's (1990) bedload transport equation. An approximate sediment budget was developed to characterize analysis segments within the reach regarding their deposition or erosion tendencies,

and use that knowledge as a guide to the type of project that may or may not succeed in the segment. For example, fish habitat structures constructed using large wood would not be expected to succeed in an analysis segment that was predicted to strongly experience a net gain in sediment over time, because the structures would have a higher risk of burial or abandonment by the river.

The sediment budget was computed for each flow and analysis segment by estimating sediment transport rates at the bounding upstream and downstream HEC-RAS cross-sections, and applying a mass balance equation for bed elevation change between transects as a function of estimated input and output bedload mass transport rates per unit width (q_B), active width (W), distance between transects (L), sediment density (ρ_s), and porosity (P) (DeVries 2000):

$$Y_T = \int_{t1}^{t2} \frac{\partial Y}{\partial t} dt \cong -\sum_{t1}^{t2} \left[\frac{(q_B W)_{out} - (q_B W)_{in}}{0.5L(W_{in} + W_{out})\rho_s (1-P)} \right] \Delta t \qquad (1)$$

where the incremental change in bed elevation ($\partial Y/\partial t$) was evaluated for each simulation flow and then multiplied by the histogram time increment (Δt) over which the modeled flow occurred during the 50-year period (cf. Figure 5). This was repeated for other flows, and the results summed to estimate a net mean change in bed elevation Y_T between successive HEC-RAS transects. A strongly positive value of the $\partial Y/\partial t$ sum was inferred as an indication of a strong tendency towards aggradation, and a strongly negative value as an indication of a stronger tendency towards degradation.

The active width used in Equation (1) was specified as the smaller of the wetted main channel width computed by HEC-RAS and an active bottom width in the main channel as delineated in GIS from scaled aerial photographs. Length was set as the main channel distance between HEC-RAS transects.

The resolution of the HEC-RAS modeling and physical characteristics of the modeled reach were such that predictions of bed elevation change at several pairs of adjacent analysis segments were strongly negative for the upstream segment and strongly positive for the adjacent downstream segment. This phenomenon appeared to reflect locations where the river flow was predicted to experience substantial energy losses due to channel expansion or contraction and directional changes in flow. The HEC-RAS model hydraulic predictions at these locations were characterized in turn by relatively irregular longitudinal trends in velocity and Froude number

over short distances. To resolve this, the two analysis segment predictions of bed elevation change were combined using the following weighted formula based on computing total volume between three successive transects consecutively numbered 1, 2, and 3:

$$Y_{T1-3} = \frac{Y_{T1-2}L_{1-2}(W_1 + W_2) + Y_{T2-3}L_{2-3}(W_2 + W_3)}{L_{1-2}(W_1 + W_2) + L_{2-3}(W_2 + W_3)} \quad (2)$$

Seven aggradation/degradation potential classes were developed subsequently and used to characterize deposition trends based on the sign and magnitude of the predicted bed elevation change (Table 2). Each analysis segment was classified accordingly and the results depicted graphically in ARC-GIS.

Table 2. Predicted bed elevation change rate and sign used to classify analysis segments according to sediment transport and deposition characteristics in the South Fork Stillaguamish River between Canyon Creek and the North Fork Stillaguamish River.

Aggradation/Degradation Potential Class	Bed Elevation Change Rate (ft/yr)
1	< −1.0 (Extreme Degradation Potential)
2	−1.0 to −0.20 (High Degradation Potential)
3	−0.20 to −0.05 (Moderate Degradation Potential)
4	±0.05 (Minor Change)
5	0.05 to 0.20 (Moderate Aggradation Potential)
6	0.20 to 1.0 (High Aggradation Potential)
7	> 1.0 (Extreme Aggradation Potential)

2.3 Aerial Photograph Interpretation

Channel features were digitized from aerial photographs, spanning 1955, 1965, 1969, 1974, 1978, 1984, 1991, 1998, 2001, 2003, 2006, and 2007. The photographs were mosaicked and georeferenced. The reach was divided into 'analysis segments' using hydraulic modeling transects as boundaries (a few transects were added later in the HEC-RAS model, but the analysis segment boundaries were preserved for consistency throughout the analysis). This permitted a common framework for synthesizing the results from the various analyses. Spatial and temporal patterns in channel migration rate and gravel bar area were derived from the aerial photographs to infer relative stability of specific analysis segments of the analysis reach associated with varying geomorphic activity levels. The 1969, 1978, 2001, and 2003

photographs were digitized but were not included in quantitative analyses so that average rates would be calculated over roughly similar time intervals.

2.3.1 Historic Channel Planform Mapping

Right and left river bank locations were digitized by the SWM GIS staff for each year of photographs. The main channel and visible side channels were mapped. The resulting digitized poly lines were overlaid chronologically and locations compared between consecutive sets of photographs. Migration rates were estimated as the local average offset distance within an analysis segment between successive main channel river bank traces, divided by the number of years between the two sets of photographs. The calculated migration rates were used as the basis for classifying an analysis segment according to planform changes, using rates established in previous analyses for the Skykomish and Sauk rivers (Table 3). The riverbank with the greater average annual migration rate was used to classify a segment.

Table 3. River channel migration rate classification for assessing channel planform changes. Migration may be to either left or right bank directions.

Planform Change Index	Average Migration Rate (ft/yr, one or both banks)
1	< 15 (minor change/measurement error)
2	15-30 (small change)
3	30-80 (moderate change, wandering tendency)
4	>80 (severe change, braiding tendency)

2.3.2 Gravel/Sand Bar and Side Channel Area Mapping

Exposed, unvegetated (i.e., active) main channel gravel/sand bar and clearly visible active side channel areas were digitized from the aerial photographs as discrete polygons. Most bars were point bars. Mid-channel bars were also mapped at specific locations where the channel widened substantially so that flow depth was very shallow across the hydraulic control formed by depositing coarse bedload. The area of gravel bar mapped in each segment was then computed and summed cumulatively from upstream to downstream in ARC-GIS to reflect the direction of sediment transport and deposition. A running sum was computed for the main channel; separate sums were computed for side channels visible on the aerial photographs, with the river mile determined by the location at which the side channel branched off from the main channel.

Not all of the aerial photographs were taken at similar flows, and differences were expected in gravel bar areas due to differential inundation. An adjustment was performed by calculating an average active gravel bar cross-channel width (W_{GB}) as the segment area digitized divided by segment centerline length, and determining an average wetted width (W_W) across upstream and downstream segment boundaries, at each flow in GIS. The photograph year with wetted widths falling in the middle of the other years (1965) was used as a reference wetted width (W_{Wref}), and wetted widths from all other years used to adjust the respective year's value of W_{GB} to an estimated equivalent reference year width (W_{GBref}), via the following formula:

$$W_{GBref} = W_{GB} + (W_{Wref} - W_{ref}) \quad (3)$$

Resulting values less than zero were set to zero. The adjustment effectively converted measured gravel bar widths (W_{GB}) to the equivalent width for the flow at which the 1965 photographs were taken (W_{GBref}).

The mean adjusted (or equivalent) widths allowed for making comparisons across different years without the influence of changing thalweg lengths (e.g., associated with channel migration). Locations were identified where mean widths changed by more than 60 ft between photographs, indicting a substantial change in storage and erosion activity. This threshold value approximates the upper limit to average correction in gravel bar width for each set of sequential aerial photographs, and thus filtered out potential instances of interpretation and measurement error. Each analysis segment was classified according to whether or not a substantial change in mean width of active bar or side channel slope occurred, and whether the change represented an overall decrease or increase in area between successive photographs. The resulting classifications were coded for each analysis segment and presented spatially in GIS format.

2.4 Avulsion Risk Assessment

Avulsion risk was assessed using LiDAR topographic data, HEC-RAS flood modeling results, and various GIS data. Factors evaluated as contributing to the potential for avulsion included the presence of concentrated flow pathways evident on the topographic surface, the average slope of pathway segments, the general flow level at which the upstream inlet would be inundated, and the inherent erosivity of soils associated with the pathway. Potential factors that could reduce the risk of avulsion were also identified, including vegetation and the presence of infrastructure. The methods used to characterize and identify these various factors are described below.

2.4.1 Individual Avulsion Risk Factors

Flow Paths: Potential avulsion pathway segments were traced on 2 ft contour maps generated from the 2006 LiDAR data as linear features with elevations that were generally lower than the surrounding floodplain. Segments began and ended at the main river channel or junctions with other segments. A GIS layer was then constructed by Laura Audette (SWM GIS staff) that depicted each potential pathway segment as a linear feature.

Inundation Flow Level: The elevation of pathway segments branching from the river was used to estimate the return interval event at which each segment and connected segments downstream and upstream would become wetted, using water surface elevations estimated for the 2-year, 10-year, and 100-year event based on the HEC-RAS modeling. Segments below junctions with upstream segments were assumed to be connected at the same level as upstream segments as long as there was no significant break in slope evident on the map downstream. For example, if a downstream segment was connected to two upstream segments with one flowing at the 2 year flood level and the other at the 10 year flood level, the downstream segment was assigned a 2-year flood level risk.

Slope: A longitudinal profile for each pathway was developed by extracting elevation data from a DEM for selected points spaced 100 ft apart along each segment. Average slope was calculated as the average of slopes calculated between points, for each segment. Slope between points was calculated as the difference in elevation between points divided by the length between points (100 ft or shorter, depending on the total length of the segment).

Soil Erodibility: The avulsion pathway layer was overlaid in GIS on a soils map produced by the NRCS. Each soil type is assigned a K_w-factor which represents both susceptibility to erosion and the infiltration rate. Soils with lower K_w-factors are more resistant to erosion due either to high clay content or high infiltration. Soils with higher K_w-factors are more erodible. Soils within the study area were classified as follows based on the NRCS K_w-factor, with greater emphasis placed on the uppermost soil horizon:

1 = K_w-factor > 0.3 (higher erodibility)
2 = K_w-factor 0.2-0.3 (moderate erodibility)
3 = K_w-factor <0.2 (lower erodibility)

Where potential avulsion pathways crossed soils with different K_w-factors, a weighted average class was calculated based on the relative length of channel crossing each soil type.

Vegetation Cover: In general, the presence of forest vegetation is anticipated to reduce the risk of avulsion, as trees provide deep, dense root masses that are more resistant to erosion and may inhibit braiding (Miall 1977). In addition, if channels do avulse through forested areas, trees that fall into the new channel provide roughness elements that reduce erosive energy and may temporarily block flow. Vegetation was assessed visually for each avulsion pathway using 2007 aerial imagery. Potential avulsion pathways were classified as forested, non-forested or open water. Only forest vegetation was considered to potentially reduce the likelihood of avulsion.

Road Grade Controls: The presence of roads can act as both a mitigating factor or exacerbate the risk of avulsion. Paved roads, and to a lesser extent gravel roads represent a "hard point" that is more resistant to erosion over the short-term. However, roads that cross avulsion pathways may also exacerbate the risk if they contain undersized drainage structures or temporarily hold back water then fail catastrophically. This analysis assumes that roads are monitored and/or protected during floods and thus moderate the risk of avulsion where they are present. Road crossings were identified from the 2007 aerial imagery. Paved roads were considered to be more resistant and more likely to be protected during floods, and thus were assigned a greater mitigative factor.

Bank Hardening: The presence of bank hardening can retard avulsion if the river does not erode around the structure and it is designed and built to counter the potential for undermining at the bank toe. Risk needs to be evaluated on a case-by-case basis, however, where type of structure (i.e., rip rap or LWD), condition of the structure, distance from the upstream and downstream ends of the structure to a floodplain swale, and respective structure end point and swale elevation differences can either be a mitigating factor or not substantially affect avulsion risk depending on the particulars of the site. For that reason bank hardening was not explicitly included as a factor in this reach-scale avulsion risk analysis.

2.4.2 Joint Avulsion Risk Factors

The factors above were considered for ways to combine them into a joint risk rating system. Weighting factors were conceived and assigned to ranges of each factor. It was decided to combine the flow level, slope, and soil erodibility factors into a weighted joint risk rating system, and apply vegetation and road characteristics as mitigating factors. Each pathway segment identified on the LiDAR topographic surface was rated accordingly, following the gradations and weightings proposed in Table 4. The joint avulsion risk was calculated for each segment as the sum of the weights assigned in Table 4 for return interval event at which the pathway may flow,

pathway slope, and soil erodibility. The following joint risk classes were then defined based on professional judgment:

- Joint Risk Weight Sum >14 = Class 1 (Highest risk)
- Joint Risk Weight Sum = 10-14 = Class 2
- Joint Risk Weight Sum = 6-10 = Class 3
- Joint Risk Weight Sum <6 = Class 4 (lowest risk)

The joint risk rating may be modified by subtracting weights for mitigating factors, with initial recommendations for weights given in Table 4. Alternatively, the mitigating factor ratings can be used on a case-by-case basis in consideration of greater site specific knowledge as to the relative importance each factor could play in mitigating joint avulsion risk.

Table 4. Summary of parameters used to assess relative avulsion risk, and the weights assigned to each parameter.

Parameter	**Criterion (weight)**			
Risk Factors:				
Flood Return Interval Causing Inundation	>100 yr (1)	100 yr (3)	10 yr (6)	2 yr (9)
Slope	≤0% (1)	0-1% (3)	1-3% (6)	>3% (9)
Soil Erodibility Class	3 (1)	2 (2)	1 (3)	
Potential Mitigating Factors:				
Vegetation	Forested (-2)	Non-Forested (0)	Open Water (0)	
Road Crossing	Paved (-3)	Gravel (-1)		
Bank Hardening Across Pathway	Rip Rap (-4)	Large Wood (-2)		

3. RESULTS

3.1 Longitudinal Profiles

The LiDAR data indicate the presence of three distinct large scale morphologic reaches, with a moderately unconfined section extending from Arlington upstream to approximately RM 6 (Reach 1), a confined section between approximately RM 6-14 (Reach 2), and a moderately confined section upstream to Canyon Creek (Reach 3; see Appendix B for a definition of confinement). The longitudinal elevation profile of the South Fork Stillaguamish River is mildly concave upstream of about RM 14 with an average gradient of 0.0031. There is a break in gradient at about RM 14, and the longitudinal profile is essentially linear downstream to the mouth with an average gradient of about 0.0016 (Figure 6). There is a second break in the profile located at about RM 6 corresponding to a change in bed rugosity (or, variability in the profile). The channel upstream of RM 6 is generally plane bed within the confined section, and closer to pool-riffle in form downstream with more defined, long wavelength pools and riffles. The average gradient upstream of RM 6 is a little steeper than downstream, approximately 0.0017 vs. 0.0015 (Figure 6).

In general, the upstream-downstream variation in bedload grain size distribution (GSD) is consistent with the morphology results, where substrates become finer in the downstream direction within the moderately confined, concave profiled Reach 3, and does not change significantly (regression $p<0.001$) in the downstream direction in Reach 1 and Reach 2 (Figure 6). The transition to a constant grain size distribution occurs at approximately RM 12. The similarity in grain size distributions suggests that the lower two reaches are generally at equilibrium grade at the reach scale, with downstream base level control provided at the confluence with the North Fork Stillaguamish R.

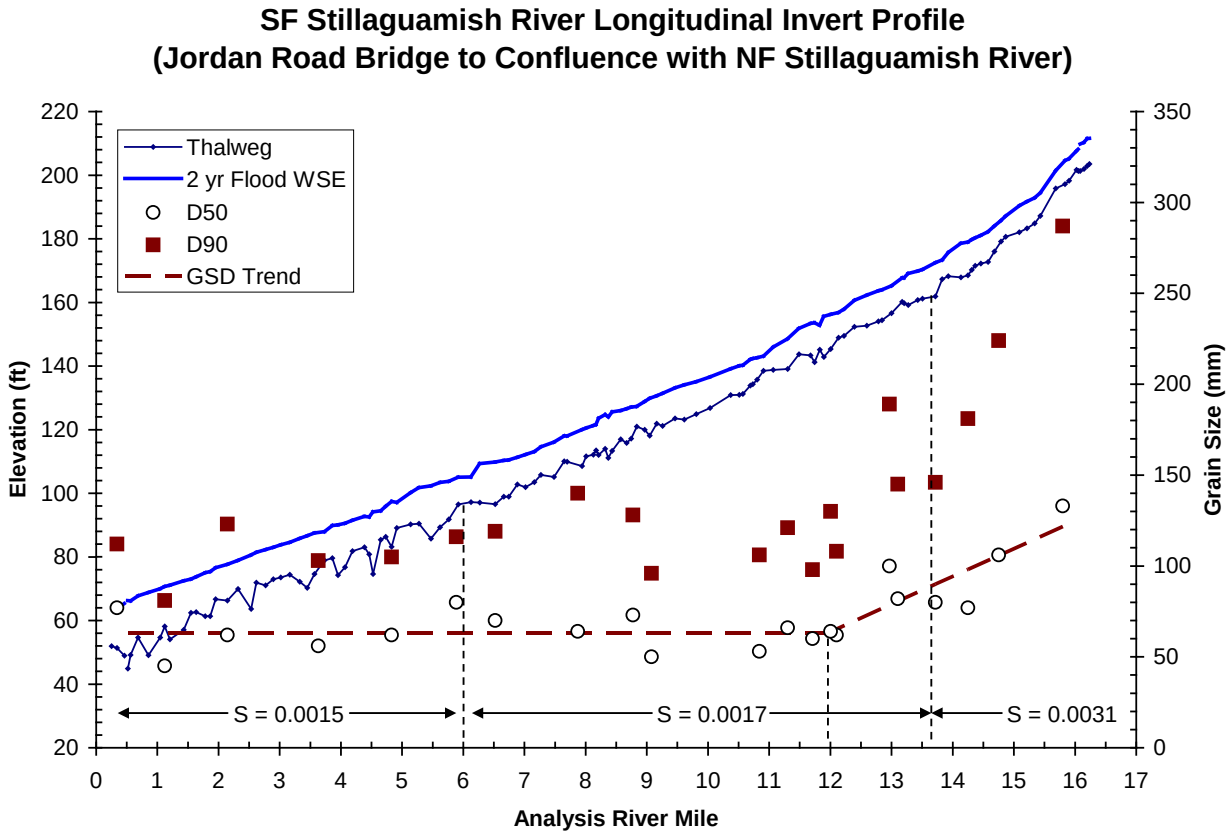

Figure 6. Longitudinal thalweg and water surface (WSE) elevation profiles and variation in selected grain size distribution (GSD) percentiles measured on depositional bar surfaces of the lower South Fork Stillaguamish River. Corresponding sub-reach breaks are indicated as vertical dashed lines based on variation in the elevation and GSD data; trendlines for GSD are also indicated by longer dashed lines.

3.2 Sediment Transport Modeling

Table 5 summarizes the estimated magnitudes of flows selected for modeling and their approximate duration. Three sub-reaches were defined with different grain size distributions for bedload transport modeling based on the longitudinal distributions depicted in Figure 5. The two upstream sub-reaches were defined based on the scatter of data points to represent an upstream coarsening trend. The pooled grain size distributions for samples collected within each sub-reach are depicted in Figure 7. Figure 7 also depicts the range of Chinook salmon and steelhead trout spawning habitat D_{50} values reported by Kondolf and Wolman (1993) in their review. The dominant bedload material appears suitable for Chinook salmon mainstem spawning in the confined and unconfined reaches below RM 14, but not upstream.

Table 5. Simulation flows modeled in HEC-RAS for the sediment transport analysis.

HEC-RAS Profile Name	Percent Exceedance	Duration (days)	Model Flow (cfs)
PF1	5	506	5410
PF2	1	268	9060
PF3	0.5	44	10800
PF4	0.4	24	11500
PF5	0.3	20	12500
PF6	0.2	18	13600
PF7	0.14 (~2-yr flood)	15	14300
PF8	0.1	11	15600
PF9	0.03 (~10-yr flood)	6	30700
PF10	0.01 (~25 year flood)	0.5	36500
PF11	0.005 (~50 yr flood)	0.5	39900

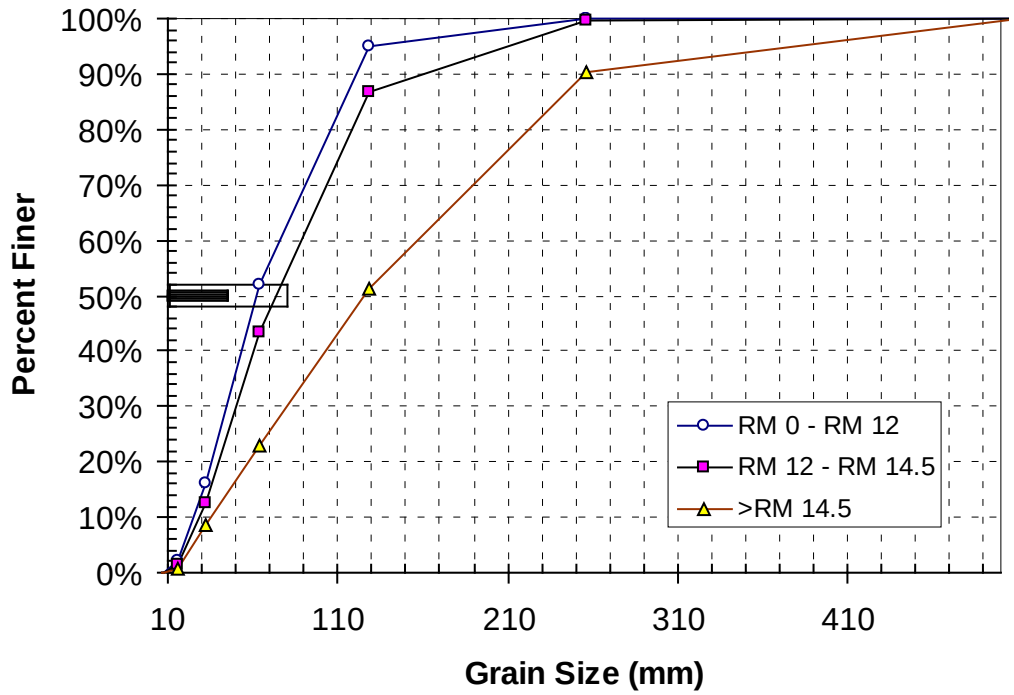

Figure 7. Grain size distributions of pebble counts collected on bedload bar deposits in the lower South Fork Stillaguamish River below Canyon Creek. Horizontal bars represent range of D_{50} values reported by Kondolf and Wolman (1993) as suitable for steelhead trout (filled bar) and Chinook salmon (open bar) spawning.

The HEC-RAS model shear stress predictions were associated with extreme variation in predicted bedload volume gains and losses across adjacent analysis segments at several locations. Smoothing using Equation (2) resulted in a more reasonable appearing plot of predicted bed elevation changes based on Parker's (1990) bedload transport equation (Figure 8). Plates 2 and 3 depict the corresponding spatial variation in aggradation and degradation potentials in the analysis reach. Some sections of the river are associated with relatively little stream-wise variation in sediment transport rates, most notably within the confined Reach 2 (RM 6-14) and the upper portion of the moderately confined Reach 3 (RM 14+). Locations with greater upstream-downstream imbalances in bedload transport potential within these two reaches appear to be localized (i) within the RM 12-14 transition zone from fining to a constant grain size distribution, (ii) in the vicinity of Trangen Meander, and (iii) in the vicinity of large, relatively small radius of curvature river bends. The upstream portions of both the unconfined and confined reaches are associated with greater spatial variation in sediment transport rate imbalance, which likely reflect effects of large scale reach transitions in channel morphology. Variability in bedload transport potential is moderate in the lower 3 miles of the river, with a local, strongly degradational trend suggested in the vicinity of the SR 530 bridge (Figure 8).

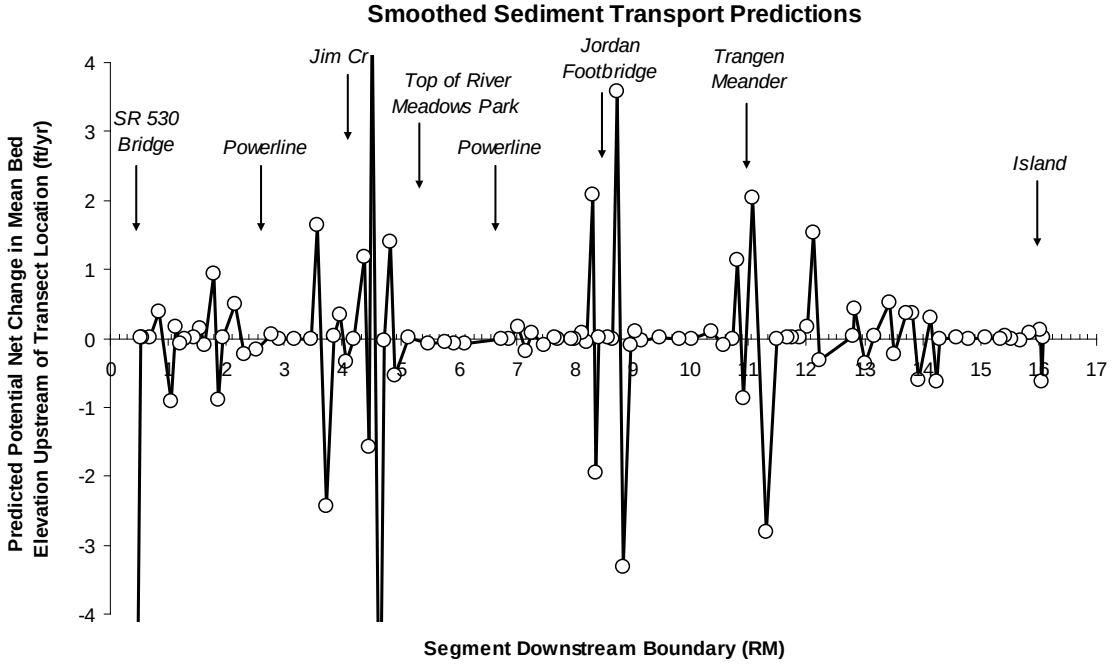

Figure 8. Longitudinal variation in predicted potential bed elevation changes within analysis segments of the lower South Fork Stillaguamish River over a 50 year period, as determined by evaluation of HEC-RAS hydraulic modeling output using Parker's (1990) bedload transport equation.

3.3 Channel Migration Patterns

The aerial photograph series provided a relatively periodic determination of channel location, with intervening periods associated with at least one large flood event occurring that exceeded the 2-year event level (Figure 9). While the South Fork gage record is incomplete for the analysis period, the North Fork gage record is complete and the occurrence of peak flow events generally tracks between the two rivers such that each aerial photograph can be assumed to reflect the occurrence of at least one bar-disturbing event after the preceding photographs were taken.

Most of the river has exhibited relatively little channel migration (Plates 4, 5). This trend is evident in the observation that the riparian vegetation along much of the river banks is composed of mature trees that appear to be relatively stable. Reaches and locations with greatest migration history generally coincide with reaches with greatest sediment transport rate imbalances. The instability at Trangen Meander is particularly notable, which reflects the tight radius of curvature imposed on the river by the valley landform. We suggest from the data that the river will continue to cut into the right bank to create a wider radius of curvature without some form of intervention. Migration rates are lowest in the confined Reach 2, but in general the river has migrated even in this reach wherever the valley bottom widens locally over the course of the aerial photographic record. Migration rates are generally largest in the lower portion of Reach 1, where there are two locations with possible upstream or downstream translation in the location of instability over time (Figure 10). The trends depicted in Figure 10 suggest that bank instability is likely to continue in segments 80 and possibly upstream, and become more focused again in the vicinity of segments 93-95.

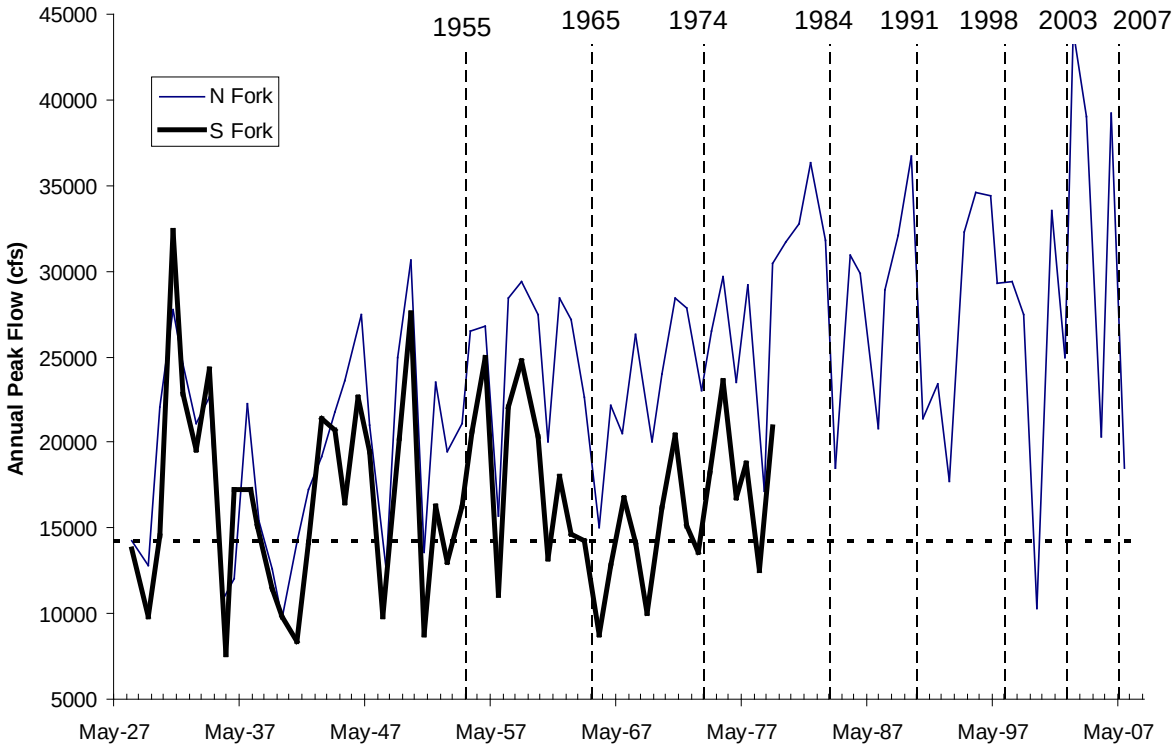

Figure 9. Annual peak flow time series encompassing the aerial photography date range, for the USGS gages in the North Fork (#12167000) and South Fork (#12161000) Stillaguamish rivers. Approximate dates when each set of aerial photographs were taken are indicated by the dashed vertical lines; the dashed horizontal line denotes the approximate 2-year flood level for the lower South Fork, which includes flows at the gage and Canyon Creek combined.

	Analysis Segment	Downstream Boundary RM	Planform Instability Index Calculated From Aerial Photogrpahy Series						
			1955-1965	1965-1974	1974-1984	1984-1991	1991-1998	1998-2003	2003-2007
Moderately Confined Reach 3	1	16.40	1	1	1	1	1	1	1
	2	16.34	1	1	1	1	1	1	1
	3	16.31	1	1	1	1	1	1	1
	4	16.28	1	1	1	1	1	1	1
	5	16.09	1	1	1	2	2	1	1
	6	15.93	1	1	1	2	3	1	1
	7	15.82	1	1	1	1	1	1	1
	8	15.69	1	1	1	1	1	1	1
	9	15.60	1	1	1	1	1	1	1
	10	15.34	1	1	1	1	1	1	1
	11	15.04	1	1	1	1	1	1	1
	12	14.82	1	1	1	1	1	1	1
	13	14.56	1	1	1	1	1	1	1
	14	14.49	1	1	1	1	1	1	1
	15	14.37	1	1	1	1	1	1	1
	16	14.17	1	1	1	1	1	1	1
	17	14.06	1	1	1	1	1	1	1
Confined Reach 2	18	13.95	1	1	1	1	1	1	1
	19	13.74	2	1	1	1	1	1	1
	20	13.66	1	1	1	1	1	1	1
	21	13.41	1	1	1	1	1	1	1
	22	13.24	1	1	1	1	1	1	1
	23	13.09	1	1	1	1	1	1	1
	24	13.04	1	1	1	1	1	1	1
	25	12.48	1	1	1	1	1	1	1
	26	12.38	1	1	1	1	1	1	1
	27	12.26	1	1	1	1	1	1	1
	28	12.14	1	1	1	1	1	1	1
	29	12.00	1	1	1	1	1	1	1
	30	11.94	1	1	1	1	1	1	1
	31	11.76	1	1	1	1	1	1	1
	32	11.58	1	1	1	1	1	1	1
	33	11.34	1	1	1	1	1	1	1
	34	11.18	1	1	3	1	1	1	2
	35	11.05	2	1	3	1	1	2	2
	36	10.91	1	1	1	1	1	1	1
	37	10.70	1	1	1	1	1	1	1
	38	10.36	1	1	1	1	1	1	1
	39	10.16	1	1	1	1	1	1	1
	40	9.93	1	1	1	1	1	1	1
	41	9.58	1	1	1	1	1	1	1
	42	9.27	1	1	1	1	1	1	1
	43	9.16	1	1	1	1	1	1	1
	44	9.08	1	1	1	1	1	1	1
	45	8.94	1	1	1	1	1	1	1
	46	8.86	1	1	1	1	1	1	1
	47	8.78	1	1	1	1	1	1	1
	48	8.68	1	1	1	1	1	1	1
	49	8.54	1	1	1	1	1	1	1
	50	8.48	1	1	1	1	1	1	1
	51	8.42	1	1	1	1	2	1	2

Figure 10. Spatial and temporal variation in channel migration tendencies within analysis segments of the lower South Fork Stillaguamish River below Canyon Creek, as indicated by successive series of ortho-corrected and geo-referenced aerial photographs. Planform change index values are described in Table 3. Arrows indicate possible stream-wise translation of instability over time.

	Analysis Segment	Downstream Boundary RM	Planform Instability Index Calculated From Aerial Photogrpahy Series						
			1955-1965	1965-1974	1974-1984	1984-1991	1991-1998	1998-2003	2003-2007
Confined Reach 2	52	8.30	1	1	1	1	2	1	2
	53	8.23	1	1	1	1	1	1	1
	54	8.11	1	1	1	1	1	1	1
	55	8.04	1	1	1	1	1	1	1
	56	7.75	1	1	1	1	1	1	1
	57	7.58	2	1	1	1	1	1	1
	58	7.36	1	1	1	1	1	1	1
	59	7.25	1	1	1	1	1	1	1
	60	7.11	1	1	1	1	1	1	1
	61	6.75	1	1	1	1	1	1	1
	62	6.59	1	1	1	1	1	1	1
	63	6.36	1	1	1	1	1	1	1
	64	6.31	1	1	1	1	1	1	1
	65	6.00	1	1	1	1	1	1	1
Moderately Unconfined Reach 1	66	5.83	1	1	1	1	1	1	1
	67	5.49	1	1	1	1	1	1	1
	68	5.19	1	1	1	1	1	1	1
	69	4.94	2	1	1	1	1	1	1
	70	4.90	1	1	1	1	1	1	2
	71	4.83	1	1	1	1	1	1	1
	72	4.70	1	1	1	1	1	1	1
	73	4.60	1	1	1	1	1	1	1
	74	4.50	1	1	1	1	1	1	1
	75	4.39	1	1	1	1	1	1	1
	76	4.22	1	1	1	1	1	1	1
	77	4.15	1	1	1	1	1	1	1
	78	3.99	1	1	1	1	1	1	1
	79	3.90	1	1	1	1	1	1	2
	80	3.76	1	1	1	2	2	2	1
	81	3.60	1	1	1	4	1	1	1
	82	3.49	1	1	1	3	1	1	1
	83	3.24	2	2	1	1	2	1	1
	84	2.93	2	1	1	1	1	1	1
	85	2.80	2	1	1	1	1	1	1
	86	2.55	1	1	1	1	1	1	1
	87	2.35	1	1	1	1	1	1	3
	88	2.17	1	1	1	1	1	1	2
	89	1.97	1	1	1	1	1	2	1
	90	1.89	1	2	1	1	3	3	2
	91	1.81	1	3	1	2	2	3	3
	92	1.65	1	3	1	1	2	4	3
	93	1.56	2	2	1	2	3	4	3
	94	1.44	2	1	1	1	1	1	3
	95	1.30	3	1	1	1	1	1	3
	96	1.22	2	1	1	1	1	1	2
	97	1.10	1	1	1	1	1	1	1
	98	1.05	1	1	1	1	1	1	1
	99	0.86	1	1	2	1	1	1	1
	100	0.69	1	1	1	1	1	1	1
	101	0.57	1	1	1	1	1	1	1
	102	0.50	1	1	1	1	1	1	1

Figure 10. Continued.

3.4 Gravel/Sand Bar Storage and Side Channel Area Trends

Figure 11 presents cumulative plots of active gravel/sand bar and side channel areas, adjusted to a common flow level, for all years of aerial photography. The differences in cumulative area between curves at a given RM reflects to some extent the time passed between the previous large flood event and the date the photographs were taken (shorter time interval → greater amount of deposit surface area that has not become vegetated yet), error in interpreting older aerial photographs (2003 and later photographs were in color; older photographs were lower resolution black and white), and error in adjusting gravel bar areas to a common flow rate.

For analysis segments where successive year's curves are approximately parallel, it may be inferred that there was probably negligible change in gravel bar storage volumes or side channel areas between the two years photographed. In other locations, the slopes of the plots differ notably, where main channel storage volumes and side channel areas either appear to have decreased or increased between successive photograph years. The rate of change in curves between successive aerial photographs may be calculated as a change in average width of active gravel/sand bar or side channel area. Segments with substantial changes in average main channel gravel bar width, and thus storage of material readily available for bedload transport, are depicted for each pair of successive photographs in Figure 12, in a format similar to that presented in Figure 10 for the channel migration results. Figure 12 represents substantial changes in gravel/sand bar area, where changes between successive photographs exceed approximately +/- 60ft.

The following observations may be made based on the data depicted in Figures 11 and 12 as follows:

- Most gravel storage occurs in the moderately unconfined Reach 1. Side channel habitat is generally absent in most of the reach and occurs primarily in the lower mile upstream of the SR 530 bridge. Area of potential side channel habitat appears to have increased most substantially in the last ten years in the mile reach upstream of the SR 530 bridge.

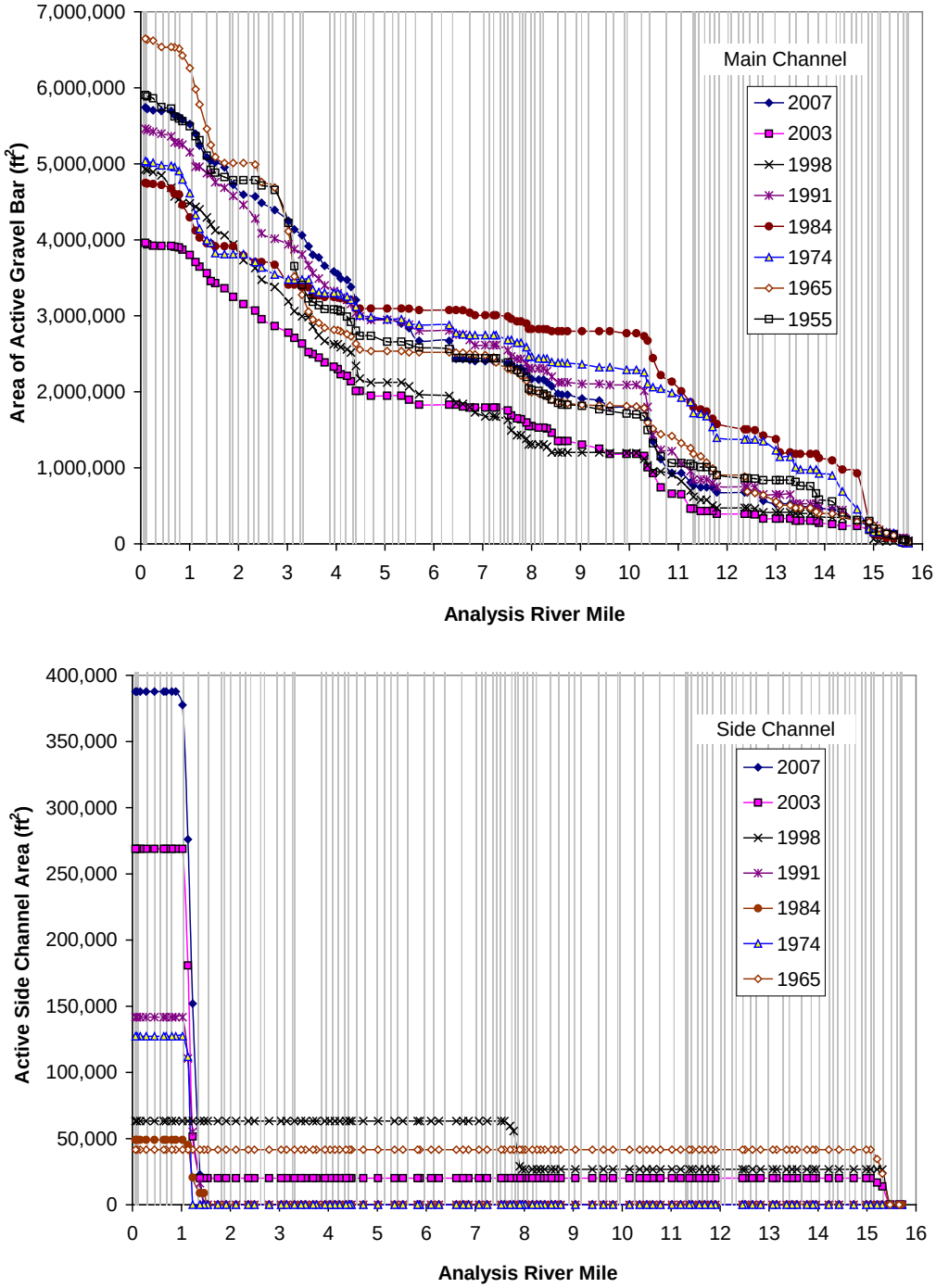

Figure 11. Cumulative active gravel/sand area mapping results digitized from aerial photography. Results are presented separately for unvegetated gravel in the main channel (top graph) and area of active side channels (bottom). The locations of the HEC-RAS transects are indicated by the dashed vertical lines.

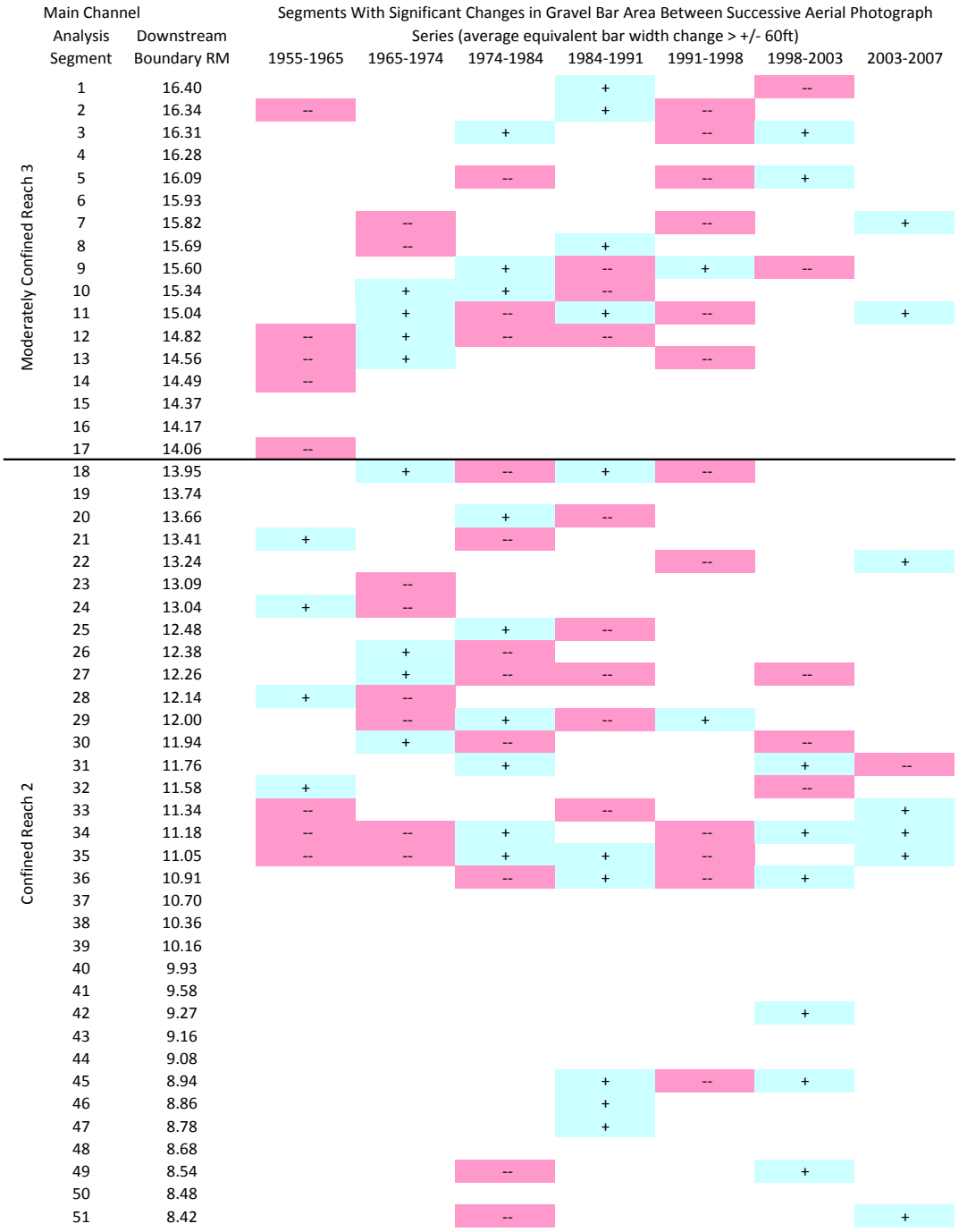

Figure 12. Spatial and temporal variation in active gravel/sand bar storage areas within the main channel for analysis segments of the South Fork Stillaguamish River, as indicated by successive series of geo-referenced aerial photographs. Change is represented as a substantial gain (+) or loss (--) in mean width of non-vegetated bar surface in excess of +/- 60 ft.

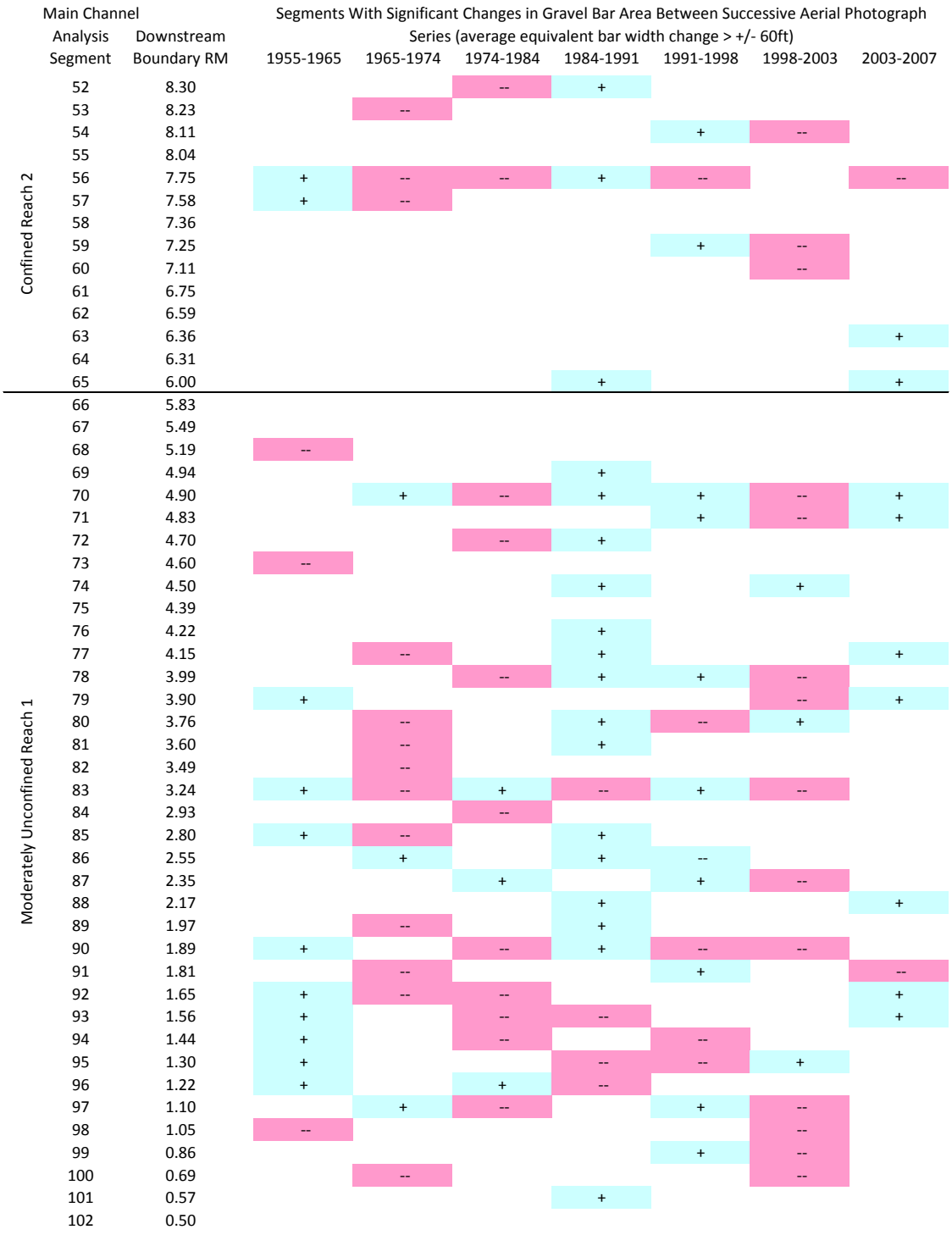

Figure 12. Continued.

- The confined Reach 2 stores relatively little gravel and acts primarily as a transport reach except at isolated locations such as Trangen Meander. Most changes in gravel storage in the reach occur upstream of the meander, and there are few opportunities for extensive bar formation downstream until the river valley opens into the moderately unconfined Reach 1. In the confined and moderately confined reaches, side channels exist in association with mid-channel islands. Changes in gravel storage occur at different times at different locations within Reach 2, where one location may exhibit a loss and another a gain between one set of consecutive aerial photographs, and the reverse in the successive set of photograph series. This suggests that storage in specific gravel bars is generally short term in the reach.

- Locations with greatest gravel bar accretion and depletion activity appear to be translating gradually in the upstream direction in the moderately confined Reach 3. However, changes in gravel bar storage in the reach have been relatively less extensive in the past ten years.

3.5 Avulsion Risk

Plates 6-8 depict the individual avulsion risk factor ratings for each delineated pathway segment. Plate 9 depicts the joint avulsion risk rating based on flow level, slope, and soil erodibility. Plates 10 and 11 depict the ratings for the vegetation and road mitigating factors. The individual and joint ratings represent relative risks amongst all potential flow paths based on physical characteristics known to affect the likelihood of avulsion. These risk ratings cannot be used to predict exactly where the channel will move during future storm events, but can be used to prioritize alternatives to reduce the risk of failure, or of potential impacts to property and infrastructure.

The results depicted in Plates 6-11 are based on LiDAR data collected in 2006 and hydraulic data collected in December 2009. Specific ratings may change in the future depending on flooding and future channel migration. It is not feasible to update the ratings each year after flooding because of the expense, however the ratings resulting from this analysis can still be used to assess general risk as described below, and provide an indication of relative differences in avulsion potential for possibly the next 10+ years.

In general, there are relatively few potential avulsion pathways evident in the topographic data, with most occurring in the unconfined Reach 1 and fewest in the confined Reach 2 (Plate 9). Of these, there are few pathways classified as joint risk Class 1 that would be expected to have the most immediate risk of avulsion in the near future because they are connected frequently at relatively low flood levels, tend to have steeper slopes, and may have more erosive soils. Class 1

pathways tend to be short in length, located across the inside of bends, and are most vulnerable to inundation at the 2-year flood level. Class 2 segments are distributed more broadly across the floodplain and are more typically associated with inundation at the 10 year flood level. In general, the farther these two class segments are situated from the main channel, and the longer the total avulsion flow path, the lower the long term risk. Most of the pathways designated as Class 1 (i.e., highest risk) represent areas that the river has occupied at one time or another during the period spanned by available historic aerial photos. Class 2 segments would likely be associated with avulsion only if specific measures were taken to increase avulsion potential, either intentionally through direct action or unintentionally through delayed maintenance or action.

Class 3 segments could become higher risk segments after the river avulses through upstream Class 1 or 2 segments. In Reach 1, most Class 3 segments are located upstream of Class 1 and 2 segments, thus limiting their avulsion potential to instances of fully developed head-cuts migrating upstream. In Reach 3, the longest potential pathways are generally rated as Class 3, and there are more Class 4 segments that have lowest relative risk.

4. SYNOPSIS OF ANALYSIS RESULTS AND SELECTION OF CONCEPTUAL PROJECTS

The following general patterns are indicated by the analysis results. The features indicated lead to river and fish habitat restoration projects that vary across the four primary geomorphic reaches identified, reflecting characteristic river processes and erosion/deposition risks observed at the reach scale.

4.1 Summary of Large Scale Variation in Reach Geomorphic Characteristics

Four geomorphic reaches are roughly delineated by the following three breaks in longitudinal trends of geomorphic attributes:

- ~RM 6 above River Meadows County Park:
  - Channel thalweg depth variation (bed rugosity): Greater downstream
  - Channel migration: Greater downstream
  - Aggradation/degradation potential: Greater variation downstream
  - Degree of reworking of active gravel bars in main channel: Greater downstream
  - Slope: Slightly lower downstream
  - Channel confinement: Less downstream

- ~RM 12, upstream of Trangen Meander:
  - Grain size: Graded channel (i.e., constant D_{50}) downstream, coarsening upstream
  - Aggradation/degradation potential: Greater variation upstream
  - Number and degree of reworking of gravel bars: Greater upstream

- ~RM 14:
  - Slope: greater upstream
  - Number and size of gravel bars: Fewer and larger upstream
  - Confinement: Less upstream
  - Aggradation/degradation potential: Less variation upstream

4.2 Potential Restoration Projects

Four general types of restoration projects are identified here along with the locations where they would be consistent with natural processes (Plate 12). It is important to note that the projects are

matched with existing river processes and watershed conditions, not future potential or pristine processes and conditions. It is the current geomorphic processes and conditions that will affect project performance and function over a reasonable project lifespan, which may be on the order of 10-20 years. Restoring watershed processes is generally beyond the scope of specific projects, and requires instead societal and institutional changes. At the same time, however, the projects identified below do have the potential to partially restore certain elements of natural watershed processes at the site and sub-reach scales. Channel migration and side channel connectivity projects have the greatest potential to restore natural river migration and floodplain connectivity processes, including cases where bank armoring is removed as part of the project. Erosion control and instream habitat structure projects will most directly improve instream habitat conditions. In the following, the general geomorphic characteristics promoting project success are identified for each type of project.

Riparian restoration (re-vegetation) projects are not identified, in large part because the conventional wisdom is that riparian restoration is recommended wherever possible. Such projects tend to reflect opportunities based more on land use patterns and willing land owners than on riverine geomorphic processes and conditions. In addition, riparian restoration can be integrated into each of the various project types below on a case-by-case basis.

4.2.1 Channel Migration Projects

Channel migration could be influenced for two purposes: (i) fine sediment input control where the river is eroding significantly into source banks, and (ii) juvenile salmonid side channel habitat maintenance or restoration. Suitable sites would be located where there are large upstream-downstream sediment transport rate imbalances and a strong aggradation tendency such that a structure could be constructed to facilitate local deposition and set up conditions favoring channel migration away from the deposition location. In addition, there should be a relatively high avulsion risk at select locations deemed feasible according to land ownership, and bank armoring should be absent or can be removed or modified consistent with landowner goals. There is relatively little bank armoring in the study reach, with greatest concentrations present at various locations in the moderately unconfined and moderately confined reaches (Plate 13)

For fine sediment control, the following analysis segments have reach scale conditions favoring functional structures that could lead to directing some flood flow away from eroding banks:

- Segments 31-32 and 34-36, in the vicinity of Trangen meander
- Segments 70-71 in the vicinity of River Meadows County Park

For juvenile side channel habitat, the following analysis segments have reach scale conditions favoring functional structures that could lead to directing flow into former channel locations and/or floodplain swales:

- Segments 74-75
- Segments 88-89, 91, and 94

Of these, segments 74-75 and 94 are influenced directly by bank armoring (Plate 13). Recent acquisition by the Stillaguamish Tribe of property along the right bank of segments 74 and 75 may make riprap removal feasible at that location. The riprap protecting the right bank in the lower portion of segment 94 would likely not affect the success of measures to reconnect the left bank floodplain in that and proximal upstream segments.

4.2.2 Instream Habitat Complexity Projects

The recovery plan indicates the need for river margin habitat complexity for juvenile and adult salmonids. Structures providing cover should be located in geomorphically inactive segments where sediment transport rate imbalances are minor, with negligible erosion or deposition tendency. In addition, avulsion potential should be relatively low where private property concerns exist, and projects should be sited preferentially in the lower gradient channel below RM 14 vs. the higher energy channel upstream, out of concern for longer term structural resilience. Straight reaches are best from a floater or boater safety concern, such that structures would be visible and flow patterns would not be directed at them. Accordingly, the geomorphic analysis results are interpreted to suggest the following suitable locations:

- Segments 9-10
- Segments 38-40
- Segment 55
- Segments 64-66

4.2.3 Mainstem Spawning Habitat

Given the relatively confined nature of the river and abundant gravel at various locations, no measures are suggested at this time to physically increase the quantity and quality of spawning gravel. However, given the general paucity of instream habitat structure, construction of smaller log structures or boulder fields could provide cover near suitable spawning locations. Suitability for such instream structures would be highest in segments where grain sizes are suitable for Chinook spawning (i.e., below RM 12, cf. Figure 7), aggradation/degradation potential is generally neutral, and where spawning surveys indicate most extensive use. The results from this analysis can be compared accordingly with redd surveys to identify suitable locations.

4.2.4 Maintain Island Splits

A persistent island/split channel morphology is limited in the lower South Fork Stillaguamish River in part because of the relatively confined nature of the river. This morphologic unit type provides habitat diversity, especially during high flow and it appears beneficial to fish to preserve islands where they exist. This can be accomplished by constructing apex jams at the upstream end of islands, subject to the constraint that the locations are not associated with a strong degradation or aggradation tendency where, respectively, the structure might fail or private land might become affected by increased flooding. The two locations identified in the analysis reach generally meet these criteria, thus may be suitable for this type of project. Jams could be placed specifically at the following locations:

- Segment 5
- Segment 51

4.3 Level of Confidence in Analysis and Results

The longitudinal profiles and/or variation of channel gradient, thalweg elevation, grain size, sediment transport analysis predictions of aggradation/degradation potential, channel migration rates, and size and extent of side channel changes over time, all consistently point to the four geomorphic sub-reaches outlined above. More site specific analysis and design will be required to evaluate specific projects and management actions, but the results presented here provide a quantitative estimate of reach scale hydraulic and erosion processes that will affect general suitability of specific measures. The information can be used to infer relative risk associated with different restoration activities (e.g., channel and floodplain connectivity, instream/bank stabilization structures, channel migration training, and bank revetment removal), with respect to whether projects would work against or with natural sedimentation and channel forming processes.

The level of uncertainty about each individual analysis varies depending on the type of data, and can be inferred in many cases from the scatter of data depicted in the graphs above. Specific cases are identified below:

- The flood level and sediment transport predictions should not be used to precisely delineate lateral flood extents and predict actual bed elevation changes. Limited field surveyed flood level data were used to calibrate the HEC-RAS model that involved approximately bankfull flood levels. Overbank flows were not calibrated.

- Typical sediment transport rate prediction errors range within an order of magnitude. However, the relative differences in sediment transport potential predicted for

successive transects should be preserved and not meaningfully affect the results presented in Figure 8, or erosion risk determinations based on those results.

- The river has changed course variably at different locations since the LiDAR data were collected; all channel planform, flood level estimation, and sediment transport predictions are presented here based on earlier topography. The 2007 aerial photographs and 2006 LiDAR and 2009 channel elevation data comprise the most recent physical data available. It does not appear feasible to redo the analyses reported here every time the channel moves, but the general trends seen here at the sub-reach scale should be preserved in the foreseeable future, possibly within the next 20-50 years.

- The channel migration traces are generally accurate for the main channel and major side channels. Smaller side channels not visible in the aerial photographs were delineated as part of the avulsion risk analysis using the LiDAR data. The collective digitized channel traces for the present and avulsion risk analyses should provide for a reasonable delineation of the channel migration zone.

5. REFERENCES

Chow, V.T. 1959. Open-channel Hydraulics. McGraw-Hill, Singapore.

DeVries, P. 2000. Scour in Low Gradient Gravel Bed Streams: Patterns, Processes, and Implications for the Survival of Salmonid Embryos. Ph.D. dissertation, University of Washington, Seattle, Washington.

Kondolf, G.M. 2000. Some Suggested Guidelines for Geomorphic Aspects of Anadromous Salmonid Habitat Restoration Proposals. Restoration Ecology 8(1): 48-56.

Kondolf, G.M., and M.G Wolman. 1993. The Sizes of Salmonid Spawning Gravels. Water Resources Research 29:2275-2285.

Kondolf, G.M., M.W. Smeltzer, and S.F. Railsback. 2001. Design and Performance of a Channel Reconstruction Project in a Coastal California Gravel-Bed Stream. Environmental Management 28(6): 761-776.

Miall, A.D. A Review of the Braided-river Depositional Environment. Earth-Science Reviews, Volume 13, Issue 1, May 1977, Pages 1-62, ISSN 0012-8252. DOI: 10.1016/0012-8252(77)90055-1.

Parker, G. 1990. Surface-Based Bedload Transport Relation for Gravel Rivers. Journal of Hydraulic Research 28: 417-436.

Rapp, C.F., and T.B. Abbe. 2003. A Framework for Delineating Channel Migration Zones. Washington State Department of Ecology, Final Draft Publication #03-06-027. Olympia, Washington.

Wissmar, R.C, and R.L. Beschta. 1998. Restoration and Management of Riparian Ecosystems: A Catchment Perspective. Freshwater Biology 40: 571-585.

List of Plates

Plate 9. Joint avulsion risk ratings of potential avulsion pathways characterized according to weighted sums of flood flow level, longitudinal gradient, and floodplain soil K_w erodibility factor ratings depicted in Plates 6-8. Tracings and ratings were based on 2006 topography. GIS Data available from Snohomish County Surface Water Management.

Plate 10. Avulsion risk mitigation ratings of potential avulsion pathways characterized according to whether a segment passes through forested land. GIS Data available from Snohomish County Surface Water Management.

Plate 11. Avulsion risk mitigation ratings of potential avulsion pathways characterized according to whether a segment is intersected by a paved or gravel surfaced road. GIS Data available from Snohomish County Surface Water Management. Road coverage may be incomplete and should be evaluated on a site-specific basis.

Plate 12. Locations of restoration projects identified in this assessment that address Stillaguamish River Recovery Plan goals and that are consistent with natural processes in the lower South Fork Stillaguamish River.

Plate 13. Results of a bank condition survey of the lower South Fork Stillaguamish River performed by Snohomish County Surface Water Management in 2006.

APPENDIX A
Details of HEC-RAS Calibration

S.F. Stillaguamish River WSE Calibration Summary

Calibration Flow 1 (cfs) **17800** Oct, 2009 flood

	TR		Dist (ft)		WSE (ft)		HWM		Modeled		Bend Radius			Width	Super Elevation (ft)				Vel	cal'd	Calib			
Loc	u/s TR	d/s TR	u/s TR	d/s TR	u/s TR	d/s TR	Dist (ft)	Elev (ft)	WSE (ft)	Vel (ft/s)	r_o (ft)	r_i (ft)	r_c (ft)	W (ft)	Δh_1	Δh_2	Δh_3	Ave	head (ft)	WSE (ft)	Error (ft)	X	Y	Comment
7	85245.1	84923.4	85239.0	84917.3	211.54	211.07	85174.6	210.81	211.45	10.63	1200	1100	1150	200	0.61	0.31	0.33	0.41		211.03	**0.22**			PDV map
6	84754.2		84748.1		208.92		84748.1	209.44	208.92	13.60	1200	1100	1150	200	1.00	0.50	0.53	0.68		209.60	**0.16**			PDV map
5	25942.9	25502.2	25936.8	25496.0	98.35	98.74	25584.2	98.65	98.66	9.69										98.66	**0.01**	1334396.4	432848.7	PDV map
4-2	19696.7	18829.2	19690.5	18823.0	89.49	89.19	18987.3	89.12	89.25	8.51										89.25	**0.13**	1336926.7	436396.9	On left bank
4-1	19696.7	18829.2	19690.5	18823.0	89.49	89.19	18905.2	89.48	89.22	8.97										89.22	**-0.26**	1336927.1	436478.9	On left bank
2	7546.2	6371.2	7540.1	6365.0	74.34	72.85	6647	73.76	73.21	4.13	900	800	850	490	0.31	0.06	0.17	0.18	0.27	73.65	**-0.10**	1329544.0	443371.6	On outside bank
1	5518.8	4513.5	5512.6	4507.4	71.68	70.53	5312.58	71.38	71.45	6.73										71.45	**0.07**	1328160.5	442709.6	HWM

Loc 2: HWM is located on the outside bank with direct impact of flow. Add superelevation and velocity haed to the modeled WSE for calibration.
Loc 6: HWM is located on the outside bank. Add superelevation to the modeled WSE for calibration.
Loc 7: HWM is located on the inside bank. Subtract superelevation from the modeled WSE for calibration.
Superelevation is the average of the calculated values from the three empirical equations in Chapter 16 of Chow (1969)
Loc 4-1 is about 100ft downstream of Loc 4-2, but has a HWM 0.36ft higher than Loc 4-2.

Calibration Flow 2 (cfs) **8330**

	TR		Dist (ft)		WSE (ft)		HWM		Modeled		Bend			Width	Super Elevation (ft)				Vel	cal'd	Calib			
Loc	u/s TR	d/s TR	u/s TR	d/s TR	u/s TR	d/s TR	Dist (ft)	Elev (ft)	WSE (ft)	Vel (ft/s)	r_o (ft)	r_i (ft)	r_c (ft)	W (ft)	Δh_1	Δh_2	Δh_3	Ave	head (ft)	WSE (ft)	Error (ft)	X	Y	Comment
7	85245.1	84923.4	85239.0	84917.3	208.47	207.90	85174.6	207.76	208.36	7.66	1200	1100	1150	150	0.24	0.16	0.13	0.17		208.18	**0.42**			PDV map

Calibration Flow 3 (cfs) **500**

	TR		Dist (ft)		WSE (ft)		HWM		Modeled		Bend			Width	Super Elevation (ft)				Vel	cal'd	Calib			
Loc	u/s TR	d/s TR	u/s TR	d/s TR	u/s TR	d/s TR	Dist (ft)	Elev (ft)	WSE (ft)	Vel (ft/s)	r_o (ft)	r_i (ft)	r_c (ft)	W (ft)	Δh_1	Δh_2	Δh_3	Ave	head (ft)	WSE (ft)	Error (ft)	X	Y	Comment
7	85245.1	84923.4	85239.0	84917.3	204.10	203.77	85174.6	205.67	204.03	2.21	1200	1100	1150	120	0.02	0.01	0.01	0.01		204.03	**-1.64**			PDV map
6	84754.2		84748.1		203.46		84748.1	202.36	203.46	2.50	1200	1100	1150	120	0.02	0.02	0.01	0.02		203.46	**1.10**			PDV map
5	25942.9	25502.2	25936.8	25496.0	91.99	89.58	25584.2	88.50	90.06	3.60										90.06	**1.56**	1334396.4	432848.7	PDV map
4	19696.7	18829.2	19690.5	18823.0	80.91	78.50	18905.2	78.80	78.73	2.10										78.73	**-0.07**	1336927.1	436478.9	PDV map
3	11323.2	10312.0	11317.1	10305.8	70.73	69.37	11215.9	70.60	70.59	1.90										70.59	**-0.01**	1330912.0	439186.2	PDV map
2	7546.2	6371.15	7540.1	6365.0	62.98	62.45	6647	62.80	62.58	1.24	900	800	850	250	0.01	0.01	0.01	0.01	0.02	62.58	**-0.22**	1329544.0	443371.6	PDV map
1	5518.8	4513.52	5512.6	4507.4	60.47	60.32	5312.58	60.57	60.44	0.85										60.44	**-0.13**	1328160.5	442709.6	PDV map

Loc 1: XS 3609.303 was raised by 2.00ft
Loc 2: XS 5909.373 was raised by 1.50ft
Loc 5-Loc 7: Not able to calibrate to within 0.5ft of surveyed WSEs with reasonable Manning's n values.

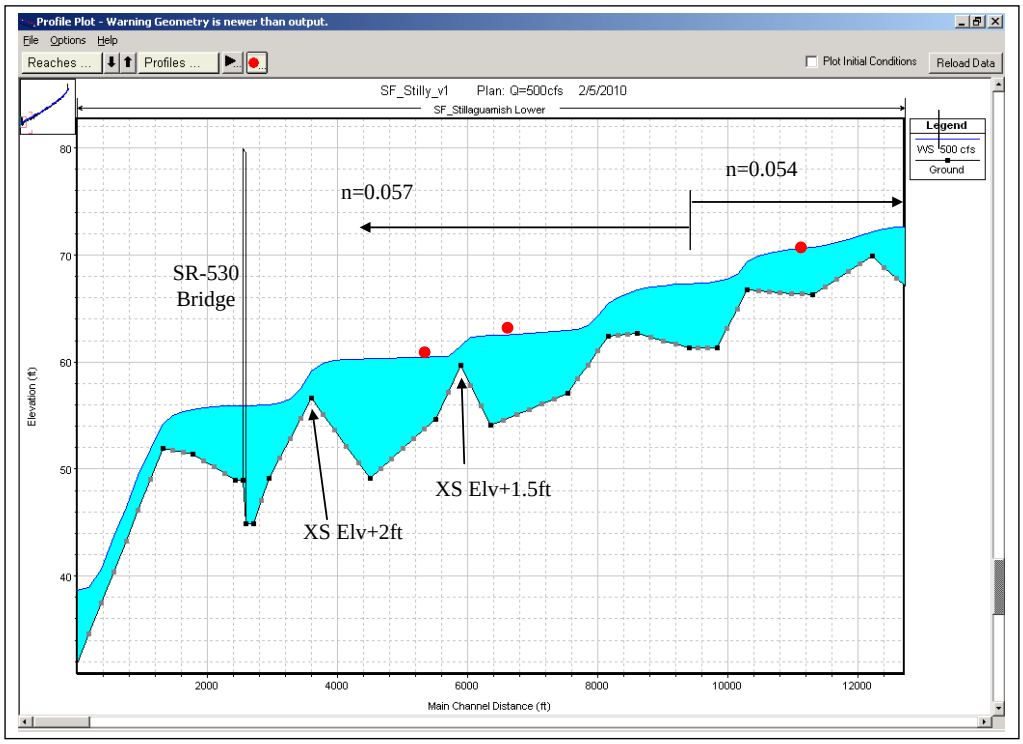

Figure A-1. WSE calibration for Q=500cfs. River distance <=12000ft. Bed elevations XS 3609.303 and XS 5909.373 are artificially raise by 2ft and 1.5ft, respectively, to achieve acceptable calibration errors. Red dots are the surveyed WSEs.

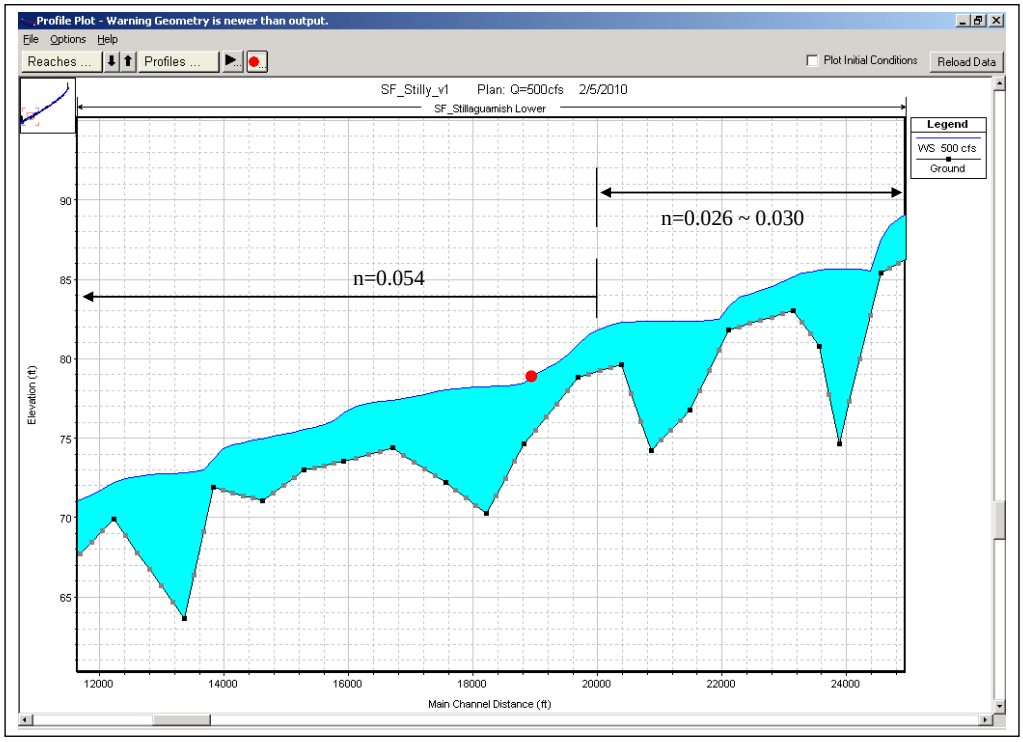

Figure A-2. WSE calibration for Q=500cfs. River distance =12000~24000ft. Red dots are the surveyed WSEs.

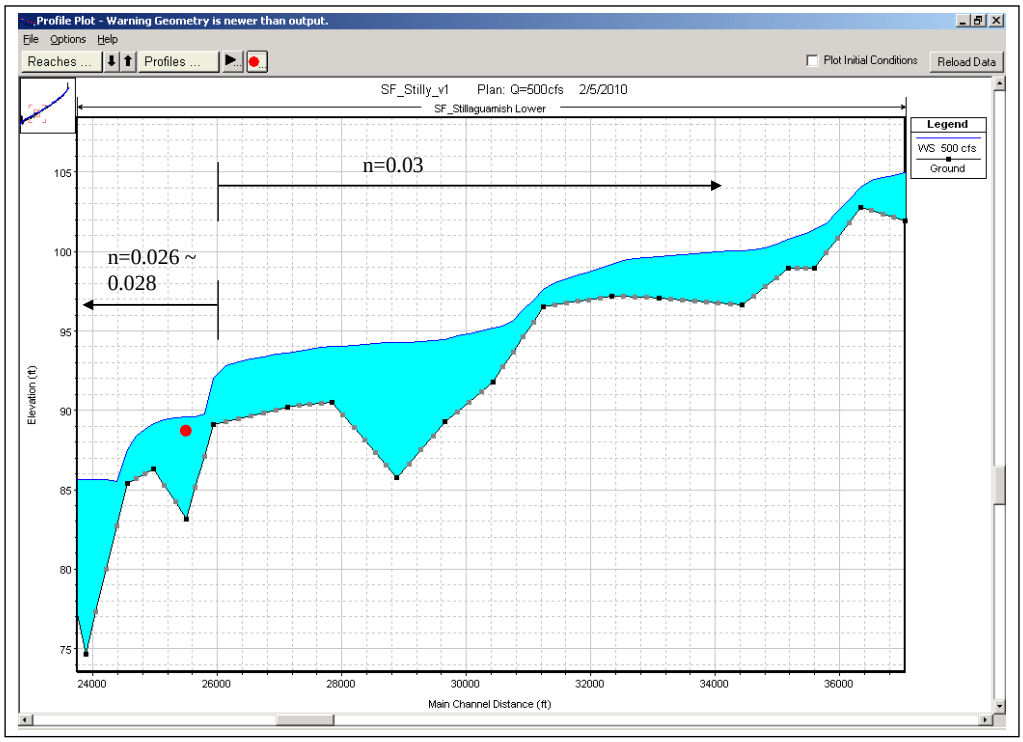

Figure A-3. WSE calibration for Q=500cfs. River distance 24000-36000ft. Red dots are the surveyed WSEs.

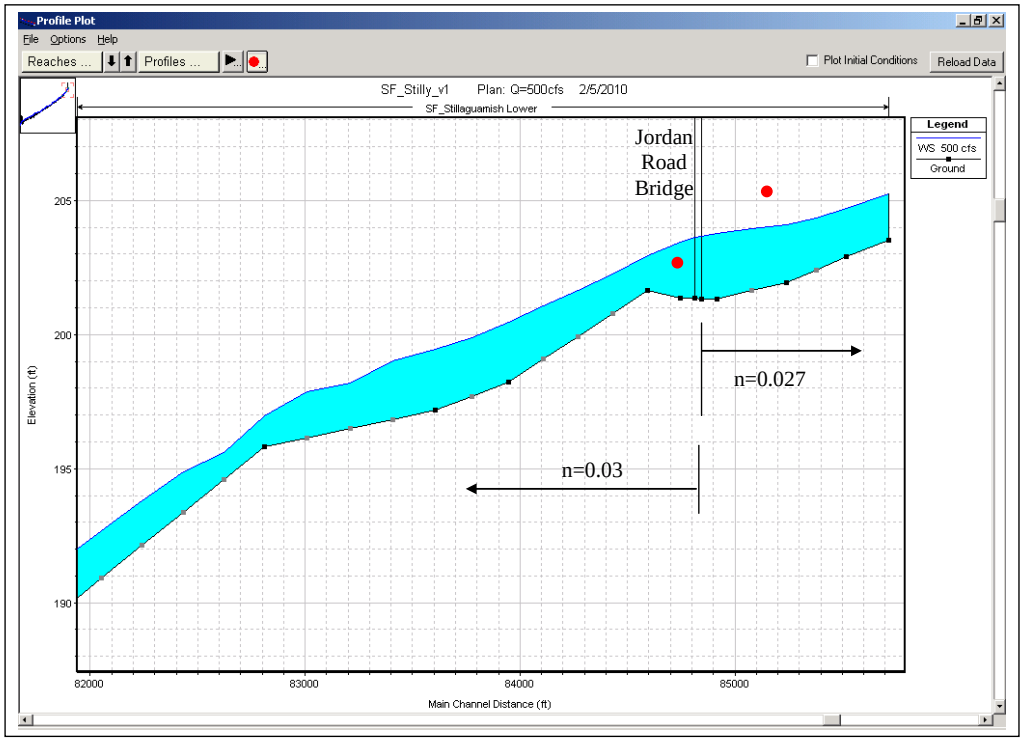

Figure A-4. WSE calibration for Q=500cfs. River distance >82000ft. Red dots are the surveyed WSEs.

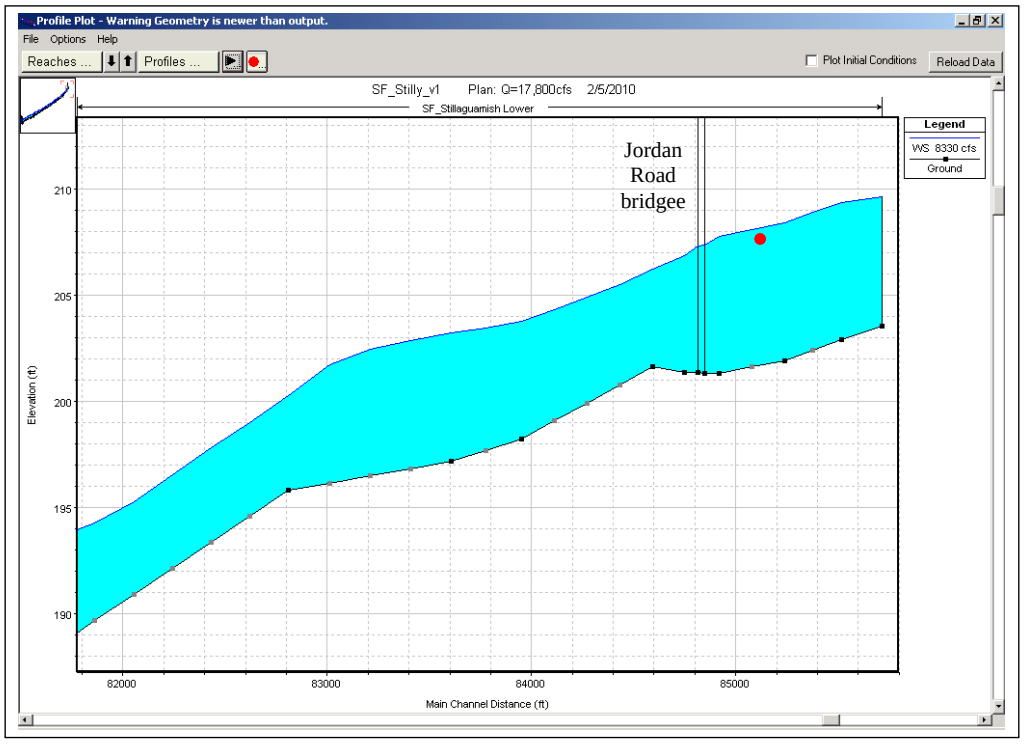

Figure A-5. WSE calibration for Q=8,330cfs. River distance >82000ft. The red dot is the surveyed WSE.

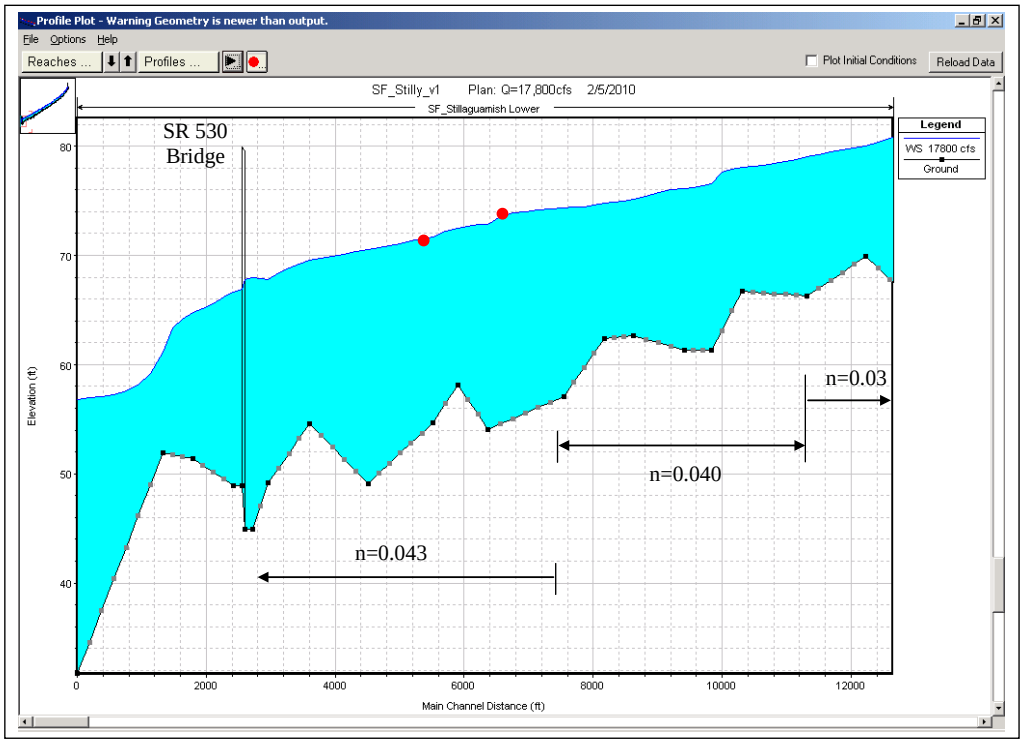

Figure A-6. WSE calibration for Q=17,800cfs. River distance <=12,000ft. Red dots are the surveyed WSEs.

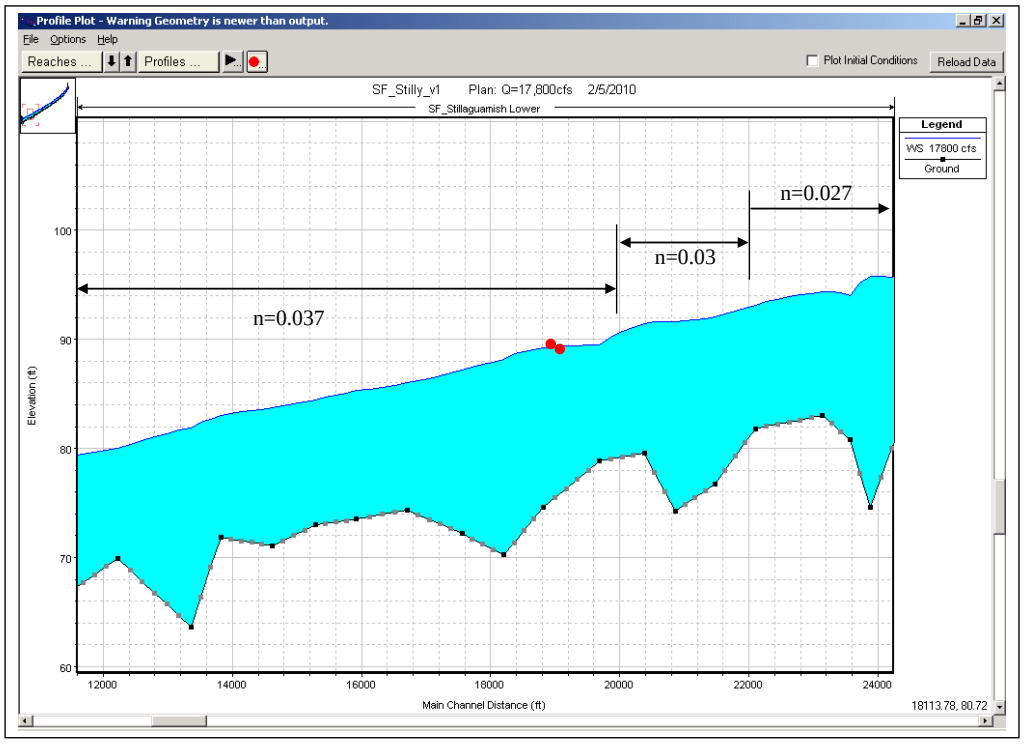

Figure A-7. WSE calibration for Q=17,800cfs. River distance 12,000-24,000ft. Red dots are the surveyed WSEs.

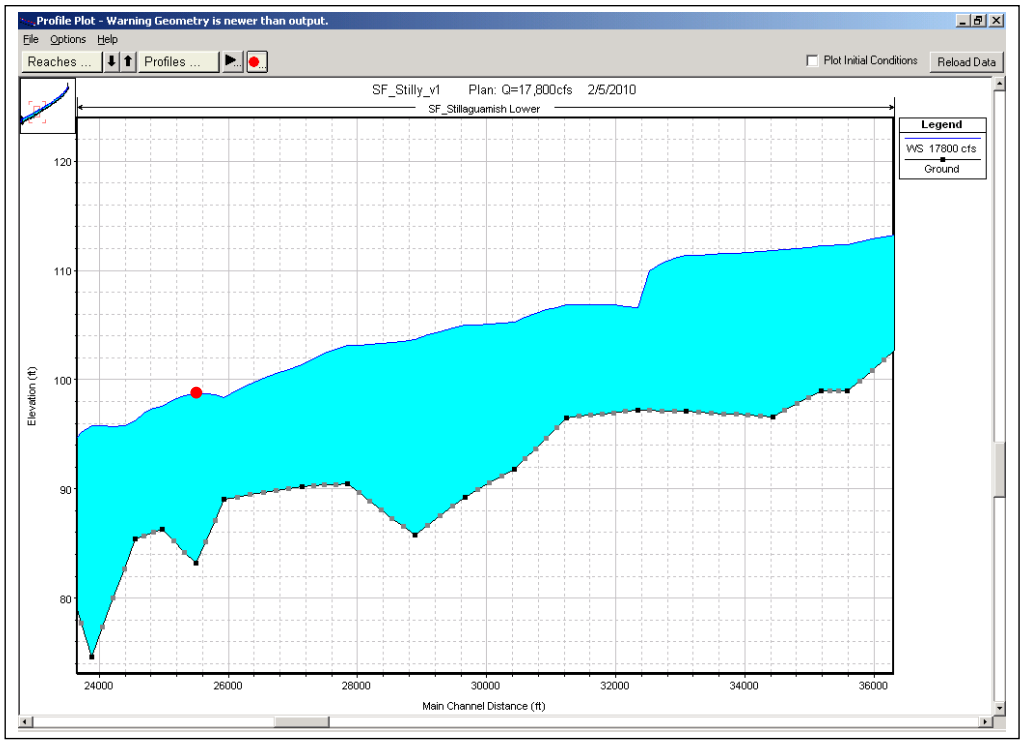

Figure A-8. WSE calibration for Q=17,800cfs. River distance 24,000-36,000ft. The red dot is the surveyed WSE.

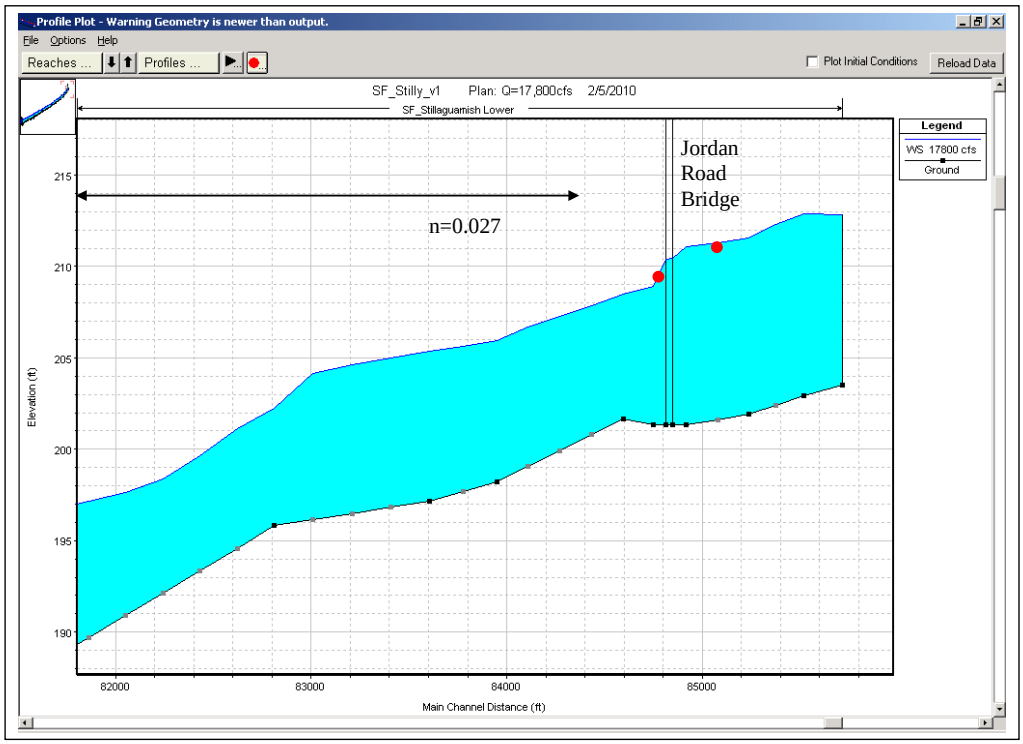

Figure A-9. WSE calibration for Q=17,800cfs. River distance >82000ft. Red dot s are the surveyed WSEs.

APPENDIX B
Definition of Channel Migration Classifications

Channel form may be classified according to degree of channel confinement by valley form, planform pattern, presence and extent of islands, types of depositional bars, and extent and character of lateral activity. The following types of channel are observed in the analysis reach, with classifications developed from Richards (1982), Leopold et al. (1995), and Galay et al. (1998):

- Confined/Meandering: Single, sinuous channel at low to bankfull flows with occasional islands and sediment deposits forming point and diagonal bars. Meander pattern sinuosity is generally contained between floodplain terraces and valley side walls. Meander migration in downstream direction is limited.
- Wandering: Channel is unconfined and free to move about floodplain. Slope is generally higher than for a purely meandering channel flowing through unconfined alluvial deposits. Planform represents an intermediate state between meandering and braided condition, with a main channel and frequent islands and small channel splits. Main channel tends to move about the floodplain through a blend of meander bend migration and channel avulsion. Abandoned oxbows or prominent arcuate swales may be present on the floodplain.
- Braided: Irregular channel pattern, with few persistent, clearly defined islands. Flow is shallower than confined/meandering and wandering channels and is distributed more evenly among many channels. Channel tends to move about primarily through avulsion process. Sediment deposits distributed throughout channel net as mid-channel bars.

The lower South Fork Stillaguamish River generally exhibits a confined nature, with some variation on the degree of confinement.